HAL open science

Development of a cementitious material for thermal energy storage at low temperature

Khadim Ndiaye, Martin Cyr, Stéphane Ginestet

To cite this version:

Khadim Ndiaye, Martin Cyr, Stéphane Ginestet. Development of a cementitious material for thermal energy storage at low temperature. Construction and Building Materials, 2020, 242, pp.118130. 10.1016/j.conbuildmat.2020.118130 . hal-02501170

HAL Id: hal-02501170

https://hal.insa-toulouse.fr/hal-02501170

Submitted on 21 Jul 2022

HAL is a multi-disciplinary open access archive for the deposit and dissemination of scientific research documents, whether they are published or not. The documents may come from teaching and research institutions in France or abroad, or from public or private research centers.

L'archive ouverte pluridisciplinaire **HAL**, est destinée au dépôt et à la diffusion de documents scientifiques de niveau recherche, publiés ou non, émanant des établissements d'enseignement et de recherche français ou étrangers, des laboratoires publics ou privés.

Distributed under a Creative Commons Attribution - NonCommercial 4.0 International License

Version of Record: https://www.sciencedirect.com/science/article/pii/S0950061820301355
Manuscript_07e50a9b414c2b915d9803d8d77ba576

Development of a cementitious material for thermal energy storage at low temperature

Khadim Ndiaye[1,2], Martin Cyr[1], Stéphane Ginestet[1]

[1]Université de Toulouse; UPS, INSA; LMDC (Laboratoire Matériaux et Durabilité des Constructions de Toulouse); 135, avenue de Rangueil; 31 077 Toulouse cedex 4, France

[2]Université de Cergy Pontoise; L2MGC (Laboratoire de Mécanique et Matériaux du Génie Civil), 5 mail Gay Lussac; 95000 Cergy Pontoise, France,

Abstract

Energy storage systems are increasingly being used to improve energy performance in industry, transport and building. The storage of energy in the form of heat is widely used in the building sector in order to increase the use of solar energy, which is necessary to streamline energy management. The storage of excess summer solar energy appears to be a solution to compensate for the thermal energy deficit in winter and to reduce the environmental and socio-economic impacts of buildings. Currently, there are several adsorbent materials capable of storing thermal energy but they use high temperature storage (around 200 °C). Ettringite is a common hydrate found in cement-based materials and has the advantage of storing energy at high density but at low temperature, around 60 °C. Portland cements used in most construction materials produce small percentages of ettringite but calcium sulfoaluminate cements (CSA) can produce much larger amounts of this compound, with fairly rapid kinetics. In this paper, the hydration of CSA-based ettringitic systems is investigated with a view to synthesizing a new heat storage material. The hydration of CSA paste samples, with and without the addition of gypsum and portlandite, constituents allowing the exclusive production of ettringite, was followed by XRD and TGA. The ettringitic system (ES1) containing CSA, gypsum and portlandite produced only 48% of ettringite with an unstable structure (swelling), so ES1 was not selected. However, the ettringitic system (ES2) containing only hydrated CSA could reach between 65% and 70% of ettringite with a very stable solid structure. In order to use the ES2 as heat storage material, it was necessary to improve its permeability, thus enhancing its storage capacity. Improving the material by foaming provided an aerated ettringitic system (AES2) with high permeability, appropriate for heat storage. This allowed the development of an ettringite-based material with high heat storage density in low temperature conditions. The heat storage prototype allowed reaching a storage density of 117 kWh/m^3 with a heat storage yield of 71%.

Keywords: Ettringite, Calcium sulfoaluminate cement, Hydration, Thermodynamic modelling, Heat storage

Abbreviations: CSA: calcium sulfoaluminate cement; ES: ettringite system; AES: aerated ettringitic system; AFt: Alumina, ferric oxide, tri-sulfate; AFm: Alumina, ferric oxide,

© 2020 published by Elsevier. This manuscript is made available under the CC BY NC user license
https://creativecommons.org/licenses/by-nc/4.0/

monosulfate, XRD: X-ray diffraction; TGA: thermogravimetric analysis; SEM: scanning electron microscope; W/C: water-cement ratio; IRH: internal relative humidity (%).

1 Introduction

Solar energy is a possible solution to reduce the dependence of the building sector on non-renewable energy. The problem of the use of solar energy is its intermittent character, that is to say, in summer solar energy exceeds the energy needed but in winter there is a thermal energy deficit. It is evident that seasonal thermal energy storage could avoid this phase shift and would increase the use of solar energy in the building sector. Moreover, materials of high heat capacity (sensible heat storage) and phase change materials (latent heat storage) are widely used in buildings for solar energy storage in the short term (day, week). However, the main disadvantage of these materials is their low heat storage density [1].

Struble and Brown [2] were among the first authors to study the storage capacity of ettringite (AFt, $3CaO.Al_2O_3.3CaSO_4.32H_2O$). This material is recognized as having a high heat storage density at low temperature (Figure 1) [3–11] and the durability and the stability of ettringite material for heat storage have been investigated [8]. The thermochemical heat storage process is based on the reversible ettringite-metaettringite conversion (dehydration-hydration process) [7,8,9]. In the charging phase, the heat is stored by endothermic heating (desorption and dehydration) and is not restored as long as the material is dry. In the discharging phase, the heat stored in the material is released by exothermic adsorption (adsorption and hydration) [5,9]. Some studies have been dedicated to the heat storage potential of ettringite [2,3,5] but many had already been done using sorption storage materials in the form of a powder bed for thermal energy storage systems of buildings [12–16]. Many experimental or numerical studies have been performed on zeolites [17–21]. These sorption storage materials are suitable for seasonal heat storage in buildings. However, their energy storage density is lower than that of thermochemical storage materials such as ettringite. The incorporation of phase change materials (PCM) in concrete walls has been widely investigated to improve building energy performance [22–28]. The PCM presence into cementitious matrix material improved its heat storage capacity and the thermal inertia of the building [28]. However, some disadvantages of PCMs constrain their use in the building sector [10]: low phase change enthalpy, unsuitable for long-term heat storage, limited storage time, mechanical effect on cementitious material, volume instability, and (in some cases) flammability of the PCM.

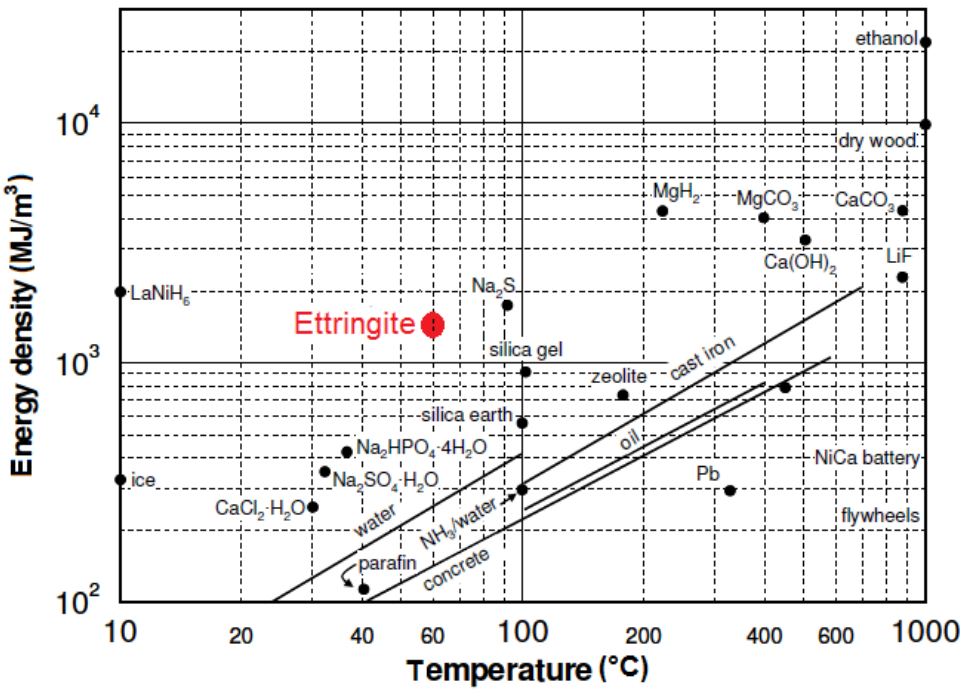

Figure 1: Energy density of storage materials versus temperature modified after Van Berkel [2,3,4,10]. Remark: data for concrete is for sensible storage.

The objective of the work presented here is to develop an ettringite based material capable of storing heat and satisfying three main criteria: (i) high AFt content to increase the heat storage density, (ii) mechanical strength to provide self-supporting capacity and (iii) high permeability to promote the exchange between water and ettringite molecules.

Pure ettringite (99% AFt) can be produced by chemical synthesis from pure minerals, thus satisfying the first criterion [29]. However, this method leads to ettringite precipitation in the form of powder, whereas monolithic storage material with a self-supporting capacity is required for the second criterion. Portland cements used in most construction materials produce small amounts of ettringite, thus Portland cement based materials do not meet the first criterion. Calcium sulfoaluminate cement (CSA) was chosen as the binder because of its high capacity for producing ettringite, with fast kinetics compared to calcium aluminate cement, e.g. [30,31]. In order to use the CSA based material as a heat storage material, its permeability needed to be increased to allow dehydration and hydration of ettringite leading to charge and discharge of heat, respectively. The foaming process was used to increase gas permeability, which would improve the exchange between ettringite and water molecules and thus the heat storage capacity (aerated ettringitic system).

To achieve these goals, the hydration of two ettringite systems based on calcium sulfoaluminate cement (CSA) was followed by X-ray diffraction (XRD), thermogravimetric analysis (TGA) and scanning electron microscopy (SEM). The first was an ettringitic system(ES1) made of calcium sulfoaluminate cement, gypsum ($CaSO_4.2H_2O$) and calcium hydroxide ($Ca(OH)_2$); and the second (ES2) contained only calcium sulfoaluminate cement. Hydration of ES2 was first modelled to predict the amount of hydrates formed at thermodynamic equilibrium and, especially, to understand the thermodynamic phenomena

(dissolution-precipitation mechanism) leading to the experimental results. This approach was complementary to the experimental monitoring of hydration. The ES2 foaming provided an aerated ettringitic system(AES2) appropriate for heat storage. These findings led to the development of a matrix that satisfied the criteria of the specification.

2 Materials and method

2.1 Materials

Several binders are able to produce ettringite, such as supersulfated cements (SSC), calcium aluminate cement (CAC) combined with calcium sulfates, or calcium sulfoaluminate cement (CSA). However, the last named system can produce higher amounts of ettringite with fairly rapid kinetics, up to 80% of ettringite by weight after 28 days, depending on its ye'elimite content ($4CaO.3Al_2O_3.SO_3$). The energy storage potential of a cementitious material increases with its ettringite content. So the choice of the storage material was founded on the hydration of two binders based on commercial calcium sulfoaluminate cement (density 2.87 g/cm^3, Blaine specific surface 5250 cm^2/g) containing 55% ye'elimite ($4CaO\cdot 3Al_2O_3\cdot SO_3$), 22% anhydrite ($CaSO_4$), 8.8% belite ($2CaO\cdot SiO_2$), 7.4% fluorellestadite ($Ca_{10}(SiO_4)_3(SO_4)_3F_2$), 3.6% periclase (MgO) and 2.3% perovskite ($CaTiO_3$). Its chemical composition is given in Table 1.

Table 1 : Chemical composition of the commercial CSA

oxide	SiO_2	Al_2O_3	Fe_2O_3	TiO_2	MnO	CaO	MgO	SO_3	K_2O	Na_2O	P_2O_5	SrO
%	5.45	25.73	0.94	0.31	0.10	40.4	3.12	21.2	0.27	0.53	0.08	0.24

Ettringite ($3CaO\cdot Al_2O_3\cdot 3CaSO_4\cdot 32H_2O$) can be with or without calcium hydroxide (portlandite) according to equations 1 and 2, respectively [32–34]:

$$4CaO.3Al_2O_3.SO_3 + 8CaSO_4.2H_2O + 6Ca(OH)_2 + 74H_2O \rightarrow 3(3CaO.Al_2O_3.3CaSO_4.\ 32H_2O) \quad (1)$$

$$4CaO.3Al_2O_3.SO_3 + 2CaSO_4 + 38H_2O \rightarrow 3CaO\cdot Al_2O_3\cdot 3CaSO_4\cdot 32H_2O + 4Al(OH)_3 \quad (2)$$

Figure 2 shows the development process allowing to obtain the aerated ettrigite system for heat storage. The hydration of ettringite systems 1 (ES1) and (ES2) according to equation 1 and 2, respectively, were investigated. This led to the aerated ettringite system suitable for heat storage.

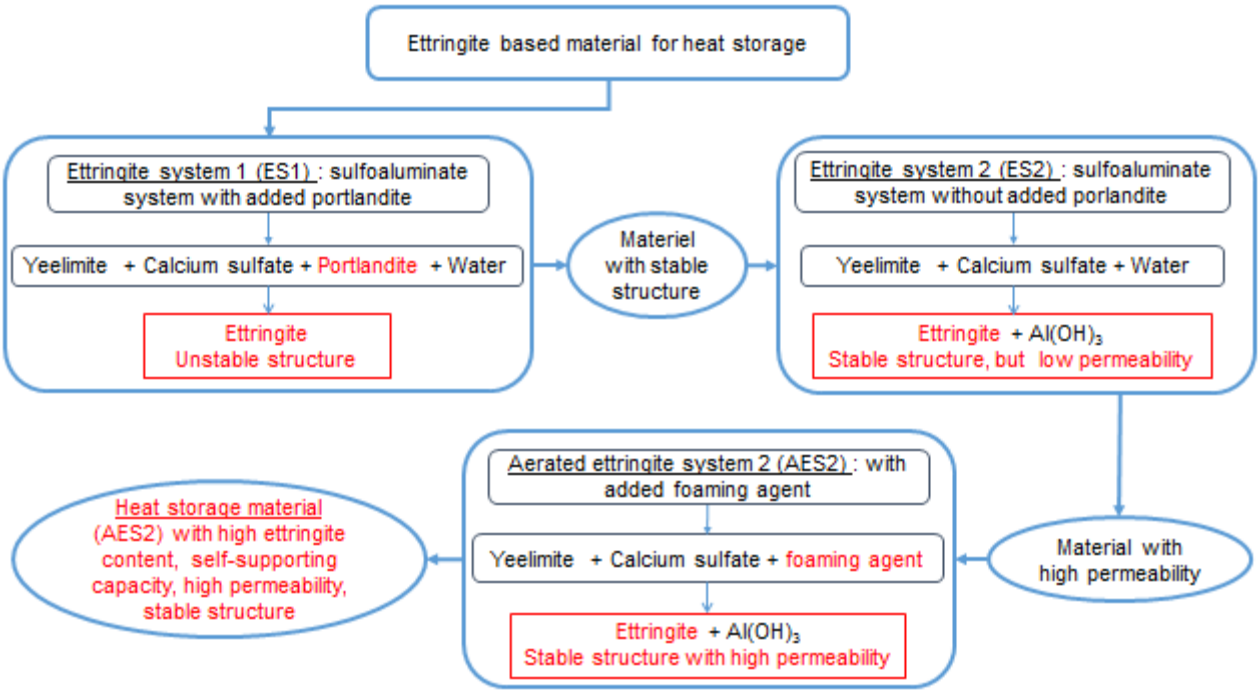

Figure 2 : Development process of ettringite based material for heat storage

2.1.1 Ettringitic systems: ES1 (ye'elimite-anhydrite-gypsum-calcium hydroxide) and ES2 (ye'elimite-anhydrite)

In order to produce exclusively ettringite and avoid coproduction of $Al(OH)_3$, the hydration of ettringitic system(ES1) according to Equation 1 was investigated. ES1 consisted of 43% CSA, 42% gypsum and 16% calcium hydroxide. The anhydrous phases (purity > 99%) gypsum and calcium hydroxide were added to the anhydrous CSA which chemical composition was provided in the table 1. The ES1 composition was calculated to reach complete hydration (with 95% of AFt) under stoichiometric conditions according to Equation 1 (Figure 2).

To avoid durability problem of the resulting ES1 paste, an ettringitic system, ES2, composed of CSA without calcium hydroxide, containing mainly ye'elimite ($4CaO.3Al_2O_3SO_3$) and anhydrite ($CaSO_4$), was hydrated according to Equation 2 (Figure 2). The water-cement ratios (W/C) of ettringite systems ES1 and ES2 were 0.6 and 0.65, respectively. These W/C were chosen to avoid segregation of the cement pastes, and also to reach the highest possible hydration under stoichiometric conditions (ettringite needs 32 moles of water per mole).

The ES2 material obtained had very low porosity (14%) and, if it was to be used as a heat storage material, its exchange surface area needed to be increased to allow dehydration and rehydration of ettringite leading to charge and discharge of heat, respectively. The ES2 was aerated by a foaming process.

2.1.2 Aerated ettringitic system AES2

There are two main methods of foaming cement pastes, (i) mechanical foaming by mixing the cement paste (and/or adding surfactants) and (ii) chemical foaming by adding a foaming agent, such as aluminium powder, the reaction of which releases gas that aerates the material, increasing its porosity. The chemical foaming method is used most often because the addition of less than 1% of aluminium powder in the paste is enough to increase its volume by a factor of 4. Moreover, this method is widely used to manufacture autoclaved aerated concrete – partly because of the simplicity of the process [35–36]. Thus the ettringitic system ES2 was aerated by addition of aluminium powder and a small amount of calcium hydroxide ($Ca(OH)_2$), the exothermal reaction of the latter releasing hydrogen gas which increased the volume of the paste and generated porosity (equation 3).

$$2\ Al + 3\ Ca(OH)_2 + 6\ H_2O \rightarrow 3CaO.Al_2O_3.6H_2O + 3\ H_2 \quad (3)$$

The resulting aerated ettringitic system (AES2) was composed of 95% ES2, 4% calcium hydroxide and 1% aluminium powder. However, it should be noted that the added calcium hydroxide was completely consumed after 5 minutes of reaction and had no influence on the CSA stability (unlike the case for system ES1). The water/cement ratio (W/C) was 1.4, i.e. higher than for ES1 (0.65) and ES2 (0.60) because the exothermic reaction of the aluminium powder on the paste (2g of water to hydrate 1g of aluminium powder) led to the evaporation of part of the water.

2.2 Methods

2.2.1 Sample preparation

To prepare the ES1 or ES2 pastes, the dry materials were first mixed to obtain homogenous mixtures. After mixing dry for 90 s at low speed, water was added according to the W/C ratio. Then after mixing for 60 s, a stop time of 30 s was taken to scrape the bottom of the mixer bowl and left to be mixed for the next 60 s at high speed. The same mixing process was used for AES2, except that low speed was used instead of high speed for the last 60 s in order to avoid removing formed foam. The resulting ES1, ES2 and AES2 pastes were cast in cylindrical (D=3 cm, L=6 cm) and rectangular (4*4*16 cm) moulds, then stored in endogenous conditions at 20 °C. After 24 h of hydration, the specimens were removed from the moulds and immersed in water at 20°C. Curing temperature and relative humidity show significant effect on the formation of ettringite. Curing under water is very benefit to the formation of ettringite [37]. The paste samples were analysed by X-ray diffraction (XRD), thermogravimetric analysis (TGA), and scanning electron microscopy (SEM). They were ground manually to 63 µm using an agate mortar in order to avoid degradation of the ettringite. Before each experimental analysis, the samples were dried at 40 °C to remove the zeolitic water without perturbing the structure of the ettringite [38]. This drying at 40 °C was completely reversible and was not considered as a decomposition phase [39,40]. The water content per ettringite molecule decreased from 32 H_2O to 30 H_2O (loss of 2 H_2O molecules per unit) without perturbing the ettringite structure [8].

2.2.2 Analytical techniques

Isothermal calorimetry (TAM Air) made it possible to follow the short-term evolution of the cement pastes by continuous measurement of the heat resulting from the exothermic hydration reaction at 20 °C. This provided some information about the hydration rate of samples at early age.

The device used for the X-ray diffraction analysis was a SIEMENS D5000 (Co Kα radiation). The specimen was irradiated by application of an electric voltage of 40 kV and a current of 30 mA, the incident angle ranging from $2\theta = 4°$ to $2\theta = 70°$ with a step size of 0.04° and a step time of 2 s.

The thermogravimetric analysis (TGA) was carried out on a NETZSCH STA 449 F3 device, equipped with an integrated thermo-balance to measure the weight loss of the heated sample as a function of time. One gram of sample previously dried at 40 °C was introduced into the platinum crucible used as the sample holder inside the high temperature oven. The sample was automatically heated from40 °C to 1100 °C at a rate of 10 °C/min. Each sample was analysed by XRD and TGA at the same age to avoid chemical evolution of the powder between analyses.

A scanning electron microscope (FEG JEOL JSM 6700F) was used to examine a transverse face of a polished sample. The sample was prepared by sawing the cylindrical specimen. Then the specimen was immersed in resin and polished after hardening. The surface to be observed was metallized using carbon. The samples were observed by SEM under vacuum with an acceleration voltage of 10 kV. The identification of the phases present in the matrix was confirmed by energy dispersive spectrometry (EDS).

The mechanical extraction of the pore solution according to the protocol described by Cyr et al. [41] and Inductively Coupled Plasma Atomic Emission Spectroscopy (ICP-AES) analysis allowed concentrations and pH to be measured in the paste pore solution after 1, 9, and 28 days of hydration (concentration of calcium, aluminium, sulfur and silicon). The ettringitic system choice was on the hydration of CSA based binders.

3 Results and discussion

3.1 Ettringitic systemES1 (ye'elimite-anhydrite-gypsum-hydrated lime)

3.1.1 Hydration and properties of ettringitic systemES1

The advantage of the presence of hydrated lime was that ettringite precipitated without any co-product such as aluminium hydroxide ($Al(OH)_3$). However, the presence of hydrated lime can lead to low hydration kinetics and to problems of durability related to the formation of expansive ettringite crystals [42].

Hydration during the first few hours

As expected for sulfoaluminate binders, the hydration reaction of ES1 began rapidly [30,31]. Figure 3 shows that the initial peak of hydration (heat flow) appeared within 1 h, which

corresponded to the initial ettringite precipitation. Then, the hydration kinetics slowed down as hydration progressed. Thus, the cumulative heat of hydration increased rapidly at the initial stage and then reached a value of 117 J/g at 72 h, which was quite low compared to that of conventional binders [30,43]. The hydration attenuation after 8h could be related to the high pH in the pore solution, due to the presence of $Ca(OH)_2$. According to Havlica and Sahu [42], the dissolution rate of ye'elimite is lower in pore solution with high pH, which leads to a deceleration of the hydration process.

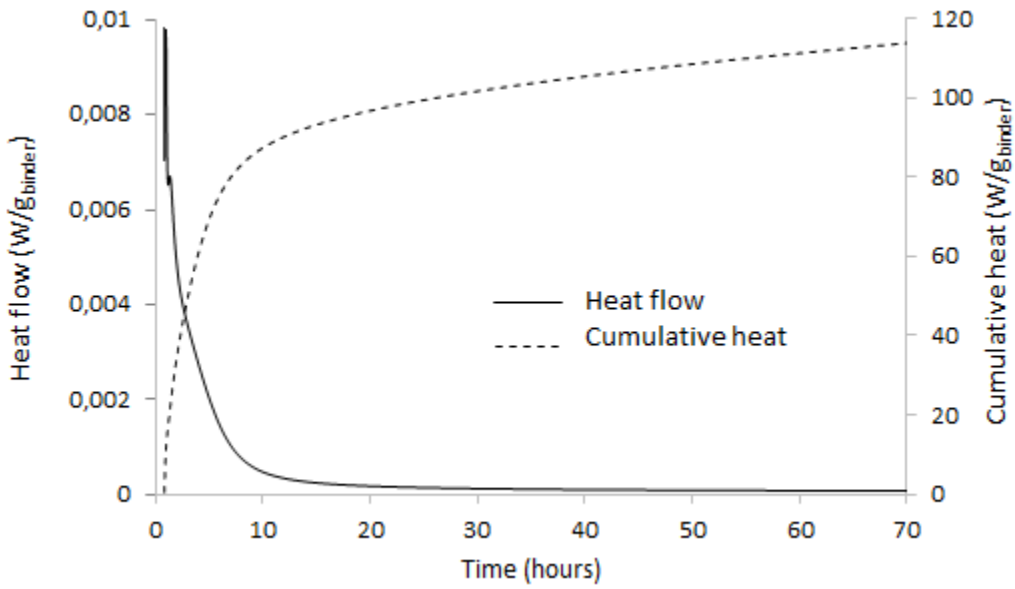

Figure 3 : Heat flow and cumulated heat of ES1 hydration

Amount of hydrate

Figure 4 shows the mass loss quantification from the TGA. An increase in AFt and a decrease in hydrated lime and gypsum was noted over the time of hydration. However, the AFt content reached a maximum of 43% at 28 days (i.e. a hydration rate of 46%), instead of 95% at theoretical complete hydration according to Equation 1. The SEM images of ES1 hydrated for 28 days confirmed the presence of non-reacted anhydrous phases (Figure 5).

This low hydration rate could be due to weak dissolution of the CSA grains, either because of a grain size effect or for reasons related to the pore solution chemistry. However, anhydrous CSA was re-ground to 7200 cm^2/g before starting hydration, thus CSA clinker grains were fine enough to react completely (no grain size effect). The low hydration kinetics noted in the ettringitic systemES1 may have been related to the pH increase in pore the solution due to the dissolution of hydrated lime ($Ca(OH)_2$) [42]. The pore solution pH reached 12.5 in 24 h.

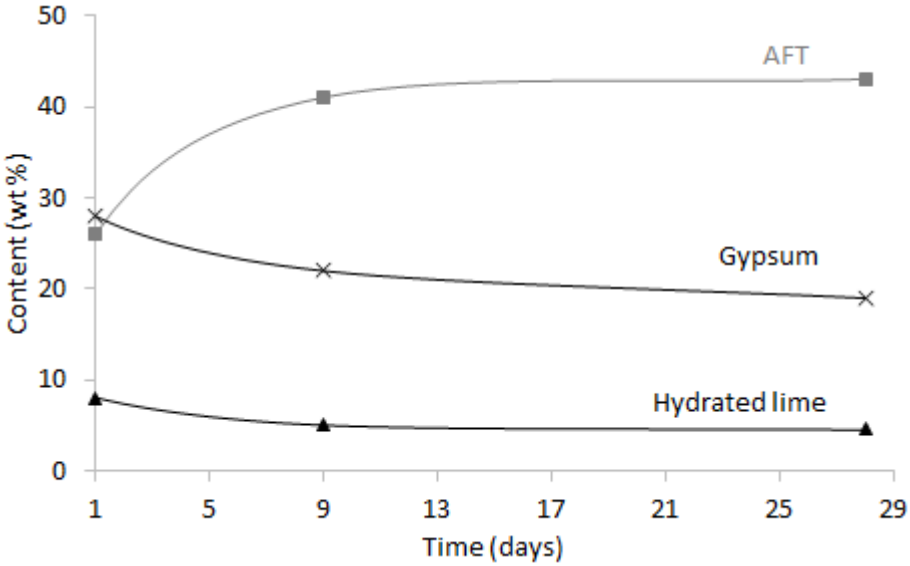

Figure 4 : Ettringite (AFt), gypsum and $Ca(OH)_2$ contents in ES1

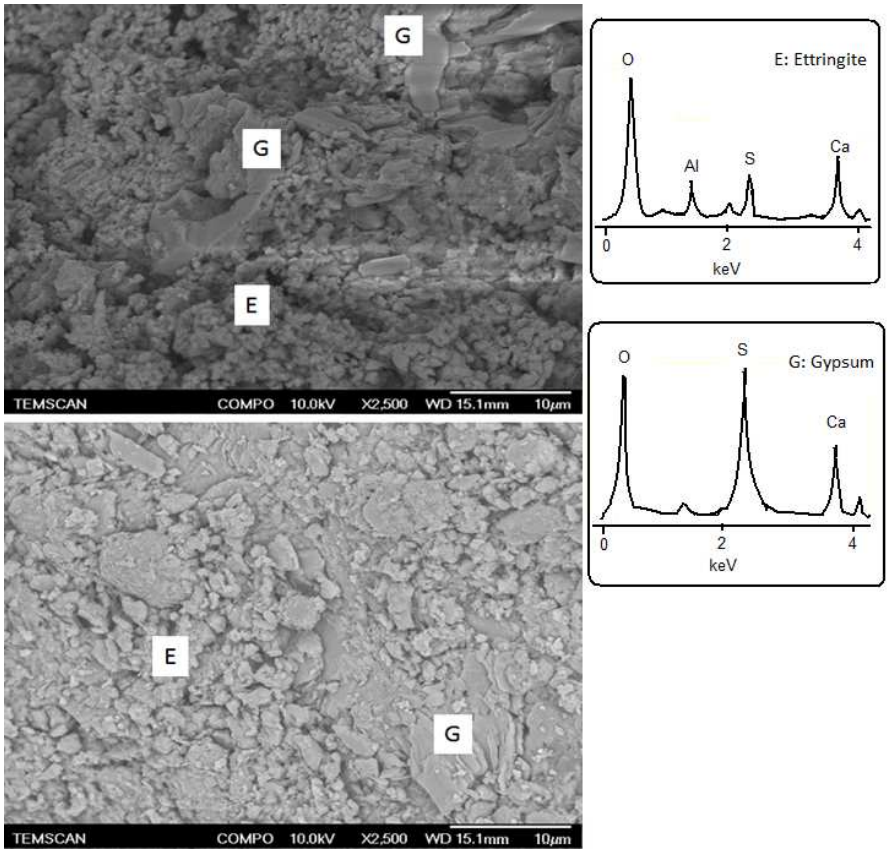

Figure 5 : SEM images of ES1 hydrated for 28 days

ES1 stability

Observation of ES1 paste samples revealed visible cracks after only a few days of hydration and the crack thicknesses increased with the hydration time (Figure 6). Volume expansion is a recurrent durability problem with ettringite materials, as the formation of ettringite in a rigid structure can generate excessive swelling. In the literature, several theories attempt to explain the expansion mechanism associated with the formation of ettringite: swelling by ettringite crystal growth [44], by water adsorption [45], or by crystallization pressure [31,46,47]. Among them, the crystallization pressure was the most plausible theory behind the expansion mechanism [31]. Lavalle [46] was the first to show the pressure due to the crystallization of salts by experiment. This theory was used to explain clearly how the ettringite precipitation led to global expansion on calcium sulfoaluminate cement or calcium aluminate cement based material [31]. It is a thermodynamic approach based on the mechanism of precipitation of ettringite from a pore solution. The possibility of ettringite crystallization in pore solution depended on its saturation index. The crystallization pressure of hydrate increased with its saturation index [48-51].

Furthermore, the volume instability could be related to the size of the ettringite crystals. Mehta et al. [45] observed large non-expansive ettringite crystals in the absence of hydrated lime and small expansive ettringite crystals in the presence of hydrated lime. The latter increased the concentration of OH^- ions in pore solution. In undersaturated lime solution with a high OH^- ion concentration, fine prismatic crystals of ettringite were formed around the aluminium particles, while large acicular ettringite crystals were produced in solution without the hydrated lime [52].

Figure 6 : Sample of ES1 hydrated for 28 days

Mechanical properties of ES1

The ettringite expansion caused durability problems of the material: macro-cracking (Figure 6) caused a drop in its compressive strength. Figure 7 shows an increase in ES1 mechanical strength to reach 8 MPa in 24 h, then a gradual fall until its bearing capacity is lost.

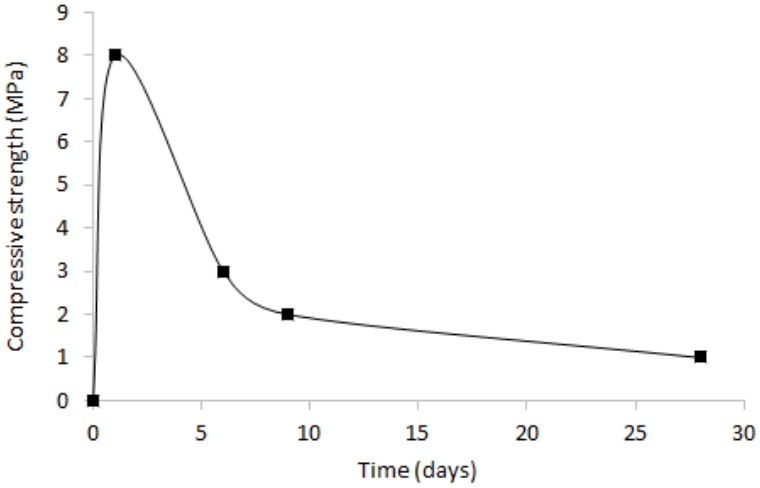

Figure 7 : Mechanical strength of ettringitic systemES1

3.1.2 Ettringitic systemES2 outcome

The ES1 paste was expected to form up to 95% of ettringite for complete hydration of the ye'elimite, in accordance with Equation 1. The experimental results showed an ettringite content of 43% after 28 days of hydration. Thus the presence of hydrated lime is thought to generate:

• high concentration of hydroxide ion (OH^-) in pore solution (high pH), which would delay the dissolution of the ye'elimite, thereby slowing down the kinetics of hydration,

• precipitation of small expansive ettringite crystals, causing swelling and cracking of the material.

Consequently, the ettringitic systemES1 was not chosen for the rest of the study because it did not meet the selection criteria for a heat storage material. To produce a cementitious material with a high ettringite content and volume stability, a CSA based material was hydrated in the absence of the hydrated lime (ES2).

3.2 Ettringitic systemES2 (ye'elimite-anhydrite)

In order to obtain a stable material with high ettringite content, ettringitic systemES2 containing mainly ye'elimite ($4CaO.3Al_2O_3SO_3$) and anhydrite ($CaSO_4$), but without hydrated lime, was tested. This binder allowed ettringite to be produce by hydration in the absence of hydrated lime according to the stoichiometric Equation 2, with a co-production of aluminium hydroxide ($Al(OH)_3$).

3.2.1 Thermodynamic modelling

Thermodynamic modelling made it possible to predict the amount of hydrates formed at thermodynamic equilibrium from the reaction of anhydrous phases. This approach was complementary to the experimental monitoring of hydration.

Modelling of CSA hydration

The Gibbs Energy Minimization Software (GEMS) is a geochemical GEMS-PSI software [53,54] based on the principle of minimizing Gibbs free energy. The evolution of the system depends on this variation of free enthalpy. The thermodynamic model does not take hydration kinetics into account because it considers only the initial stage and the thermodynamic equilibrium (i.e. the final stage of hydration).

The hydration kinetics modelling, which combined the thermodynamic model GEMS3 (version 3 of the software) and the database CEMDATA07.3, predicted the cement hydration and, especially, gave an understanding of the thermodynamic phenomena (dissolution-precipitation mechanism) leading to the experimental results. The cement-specific CEMDATA07.3 database was fed with experimental data derived from cementitious materials in the literature [55-60]. The intrinsic properties of the anhydrous and hydrated phases required for thermodynamic modelling were provided (molar volume, solubility product, etc.). This database was used to simulate the hydration of Portland cement and/or calcium sulfoaluminate cements [34,61].

In a cement paste, GEMS predicted the precipitation of hydrated phases from the dissolution of anhydrous phases, by calculating the saturation index (IS). The latter was calculated, for each mineral, from the activity of species in solution (IAP). The effective saturation index (IS_{eff}) is more suitable than the saturation index; since it takes the number of dissolved species (ions) interacting to precipitate hydrates [62] into account. In fact, the use of the saturation index was not suitable for comparing phases with different numbers of species (e.g. 15 ions for AFt and 2 ions for $Al(OH)_3$). The effective saturation index (IS_{eff}) of the mineral was obtained by dividing the saturation index by the number of ions needed to precipitate the mineral (equation 4):

$$IS_{eff} = \frac{IS}{n} = \frac{1}{n} log_{10}\left(\frac{IAP}{K_0}\right) \qquad 4$$

with n the number of ions allowing the solid to precipitate, K_0 the solubility product at equilibrium, and IAP the ionic activity product

The ionic activity product (IAP) for each solid was determined from the species activities in the pore solution. The activity of a species is the product of the concentration and the activity coefficient of the chemical species. The activity coefficient takes the influence of the surrounding ions in solution into account. It depends on the ionic strength and can be calculated according to the Debye-Huckel or the Davies model [63,64]. The evolution of the reaction (dissolution or precipitation) was deduced from the effective saturation index for each solid phase:

- $IS_{eff} > 0$ → the solution is oversaturated with respect to the solid phase,
- $IS_{eff} = 0$ → the solution is in thermodynamic equilibrium with the solid phase,
- $IS_{eff} < 0$ → the solution is undersaturated with respect to the solid phase.

This parameter (IS_{eff}) makes it possible to determine the phases that can be formed in solution, from the thermodynamic perspective [61]. Thus, the most stable hydrates will be precipitated. The composition of the cementitious material at thermodynamic equilibrium was then predicted. The mass, the volume of minerals and the pH of the interstitial solution were provided. For example, ettringite is stable due to its low solubility. Dissolution of ettringite is carried out according to equation 5 [60]:

$$3CaO.Al_2O_3.3CaSO_4.32H_2O \rightarrow 6Ca^{2+} + 2Al(OH)_4^- + 3SO_4^{2-} + 4OH^- + 26H_2O \qquad 5$$

So the effective saturation index IS_{eff} of ettringite was determined by GEMS according to equation 6:

$$IS_{eff} = \frac{1}{n} * \log_{10} \frac{IAP}{K_0}, \quad \text{with } IAP = [Ca^{2+}]^6\,[Al(OH)_4^-]^2\,[SO_4^{2-}]^3\,[OH^-]^4 \qquad 6$$

n number of ions allowing ettringite to precipitate, n = 15 ($6Ca^{2+}$, $2Al(OH)_4^-$, $3SO_4^{2-}$, and $4OH^-$)

Pore solution of ES2

Table 2 shows the concentration of calcium (Ca), aluminium (Al), sulfur (S) and silicon (Si) in ES2 pore solution after 1, 9 and 28 days of hydration. The precipitation of hydrates in the ettringitic systemwas dependent on this pore solution chemistry. A decrease of Ca, Al and S was observed as the hydration progressed. This was related to the precipitation of hydrates, such as ettringite, which consumed these chemical species. As expected, a low Si concentration was noted. This was related to the low C_2S content of ES2 (8 wt%). The effective saturation indices were calculated under GEMS from species concentrations in the pore solution measured after 1, 9 and 28 days of hydration (Figure 8). This provided the evolution of thermodynamic stability of hydrates (precipitation - dissolution) as the hydration progressed.

Table 2: Pore solution chemistry of ES2 after 1, 9 and 28 days of hydration

Time (days)	Ca (mmol/l)	Al (mmol/l)	S (mmol/l)	Si (mmol/l)	pH
1	1.28	74.50	111.50	< 0.01	11.8
9	0.69	19.61	6.69	< 0.01	12.1
28	0.31	10.89	4.40	0.03	12.3

Figure 8 shows the effective saturation indices of ettringite (AFt), AFm, amorphous Al $(OH)_3$, stratlingite, gypsum, anhydrite, portlandite and C-S-H. The oversaturation of the pore solution for ettringite and amorphous $Al(OH)_3$ between 1 and 28 days of hydration was noted in Figure 8. This proved the thermodynamic stability of these hydrates, which can precipitate and remain stable in the pore solution during the hydration of ES2. In contrast, the pore solution was undersaturated in relation to AFm and stratlingite at the first day of hydration, then

become oversaturated at the 9th day of hydration, corresponding to the delay in the formation of these hydrates compared to AFt and amorphous $Al(OH)_3$.

The solution remained undersaturated for anhydrite, even though its effective saturation index increased with the hydration time. Anhydrite was the source of sulfate ions in the ES2 pore solution and its dissolution at the beginning of hydration led to the high sulfate concentration observed after one day of hydration (Table 2). The solution was also undersaturated in relation to gypsum during hydration, which, therefore, could not precipitate.

Portlandite and C-S-H are stable hydrates (solution oversaturated) in Portland cement pastes or Portland and CSA mixtures [61]. However, these hydrates remained undersaturated during the hydration of ES2, thus predicting the impossibility of their formation in ES2.

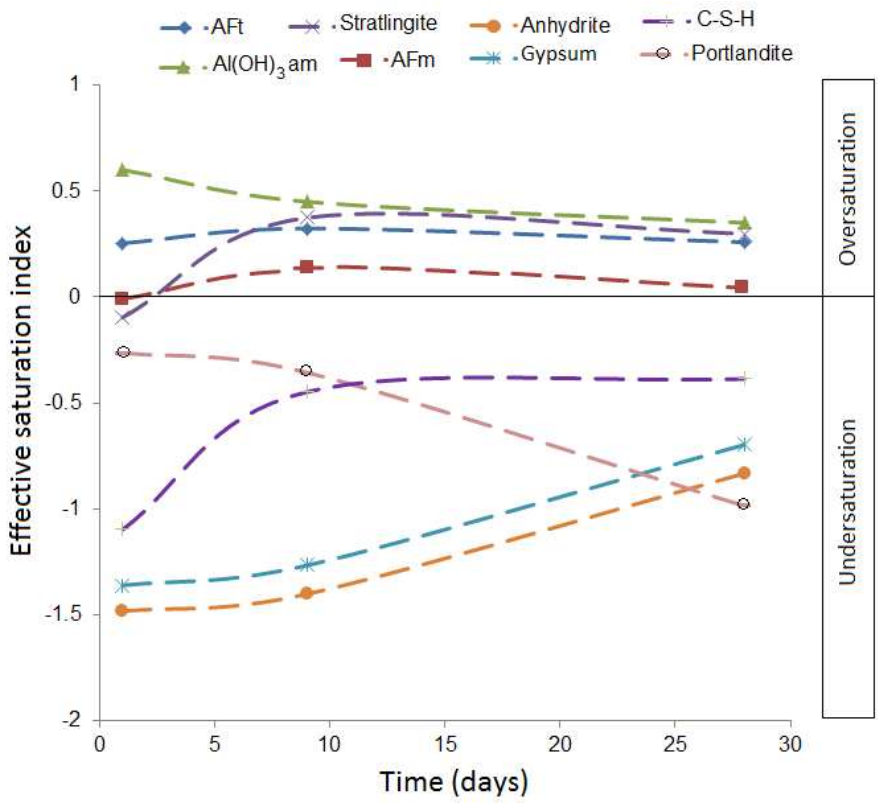

Figure 8 : Evolution of effective saturation indices in ES2 pore solution

Hydration kinetics of ES2

The GEMS software provided the results at thermodynamic equilibrium; the temporal evolution of the system was not taken into account. To obtain the hydration kinetics, it was necessary to introduce a dissolution kinetics, which provided the quantity of anhydrous over time. GEMS software again calculated the amount of hydrates formed (the most stable hydrates) from the quantity of anhydrous phases supplied (provided by its dissolution kinetics). The kinetics of hydration was obtained by considering a succession of thermodynamic equilibria over time.

Ye'elimite ($C_4A_3\bar{S}$), anhydrite ($CaSO_4$) and belite (C_2S) were the reagent anhydrous phases of the system. The dissolution kinetics of each phase was determined (semi-quantization) from the surface under their characteristic peaks in the XRD diagram, considering that this surface decreased proportionally to the quantity of anhydrous phase as the hydration progressed. The peak height was also used to determine the hydration kinetics of anhydrous phases of Portland cement [65]. The dissolution kinetics of each anhydrous phase was modelled by a kinetic function [66] (equation 7).

$$\frac{\partial m(t)}{\partial t} = K_c(m_{eq} - m(t)) \qquad 7$$

with m(t) the amount of anhydrous phase at time t, m_{eq} the amount of anhydrous phase at thermodynamic equilibrium and K_C the kinetic coefficient intrinsic to the anhydrous phase.

The analytical resolution of equation 7 gave the expression of the quantity of anhydrous phase at each instant of hydration (t) (equation 8):

$$m(t) = \frac{m_0 - m_{eq}}{\exp(K_c.t)} + m_{eq} \qquad 8$$

where m_0 is the amount of anhydrous phase at the initial time, and m_{eq} and K_c are obtained for each anhydrous phase by minimizing the difference between model and experiment by the least squares method.

Thus, the same kinetic model was used for three anhydrous phases (ye'elimite, anhydrite and belite), but the parameters m_0, m_{eq} and K_c were specific to each phase. The ES2 composition (amount of hydrated phases) over time was predicted using the coupling between the thermodynamic modelling and the dissolution kinetics of anhydrous phases. At each moment, the composition of the system was obtained by establishing a thermodynamic equilibrium from the new quantity of anhydrous in the pore solution provided by the kinetic model. Figure 9 shows the simulation results of the hydration of ES2.

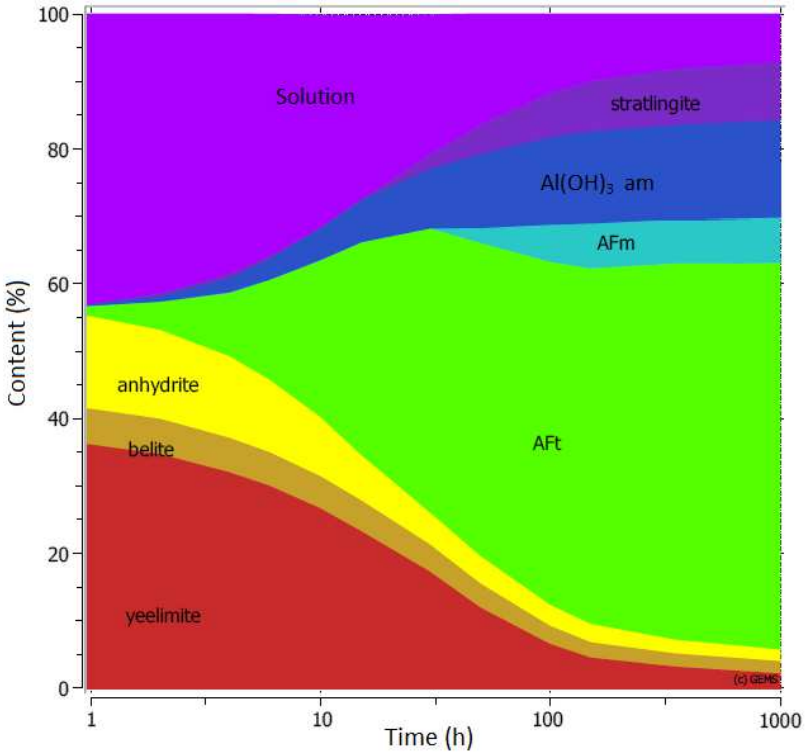

Figure 9 : Evolution of ES2 paste composition over hydration time

As expected, ettringite was the main hydrated phase and it precipitated from the dissolution of ye'elimite and anhydrite (equation 2). The amount of ettringite increased as the hydration progressed because the dissolution of ye'elimite and anhydrite was gradual and continued even until the 28th day of hydration (672 h). The amount of hydrate after 28 days was predicted with a mass content of 61% AFt (Figure 9). This value is lower than that calculated (70%) considering the stoichiometric condition according to Equation 2. This was due to incomplete hydration of the system since there were still traces of non-hydrated ye'elimite and anhydrite after 1000 h (Figure 9).

The late precipitation of small amounts of AFm seemed to be related to the decrease in the concentration of sulfate ions in the pore solution noted in Table 2, due to the high consumption of anhydrite. This sulfate deficiency drive to the ye'elimite reaction according to equation 9:

$$4CaO.3Al_2O_3.SO_3 + 18\ H_2O \rightarrow 3CaO.Al_2O_3.CaSO_4.12H_2O + 4\ Al(OH)_3 \qquad 9$$

Stratlingite was precipitated late from the amorphous $Al(OH)_3$ and C_2S formed according to equation 10. The hydration of ES2 was based on the dissolution-precipitation mechanism. Thus, the delayed precipitation of stratlingite with respect to ettringite was explained by the low dissolution kinetics of C_2S in relation to ye'elimite and anhydrite (Figure 9).

$$2CaO.SiO_2 + 2\ Al(OH)_3 + 5\ H_2O \rightarrow 2CaO.Al_2O_3.SiO_2.8H_2O \qquad 10$$

Furthermore, the form of calcium sulfate (anhydrite, gypsum or hemihydrate) had an influence on the hydration. The dissolution kinetics of anhydrite is slower than that of gypsum or hemihydrate [67]. This allows the dissolution kinetics to be regulated and gradual formation of AFt to be obtained, continuing after several days of hydration (Figure 9). The use of gypsum (or hemihydrate) instead of anhydrite as a source of CSA based binder leads to the higher AFt content at the beginning of hydration, but this trend reverses over time. Winnefeld and Lothenbach [62] observed that the CSA paste with the anhydrite reached a higher AFt content after a few days of hydration. The dissolution kinetics of anhydrite is more favourable to the continuity of the CSA hydration (after 3 days of hydration) [67]. Such modelling of the hydration kinetics allowed us to predict the temporal evolution of ES2 composition, and also to fully understand the hydration mechanism causing dissolution of anhydrous phases and precipitation of hydrates. This enabled the experimental results to be compared and interpreted.

3.2.2 Experimental monitoring of ES2 hydration

Hydration during the first hours

As with ES1, isothermal calorimetry (TAM Air) allowed the short-term evolution of ES2 paste to be followed by continuous measurement of the heat resulting from the exothermic hydration reaction (Figure 10). An initial hydration peak, attributed to ettringite precipitation from anhydrite [30], was observed after around 1 h of hydration. Then there was a period of lower activity before a second peak of hydration after 8 h. The period of low ettringite production, which lasted 7 h in this case, has already been observed in the literature [62]. The duration of this period decreased with the increase of ye'elimite-anhydrite ratio [62]. Thereafter, a third hydration peak (at 32 h) was measured, confirming the continuity of the hydration. The first two hydration peaks were attributed to AFt, but the third peak seemed to be related to the late AFm precipitation predicted by thermodynamic simulations in Figure 9. The cumulative heat showed that the hydration kinetics was low initially (compared to that of ES1 in Figure 3). However, this trend reversed after 8 h of hydration, the ES2 hydration continued with high kinetics. The heat of hydration gradually intensified to reach 315 J/g_{binder} in 70 h (instead of 120 J/g_{binder} for ES1).

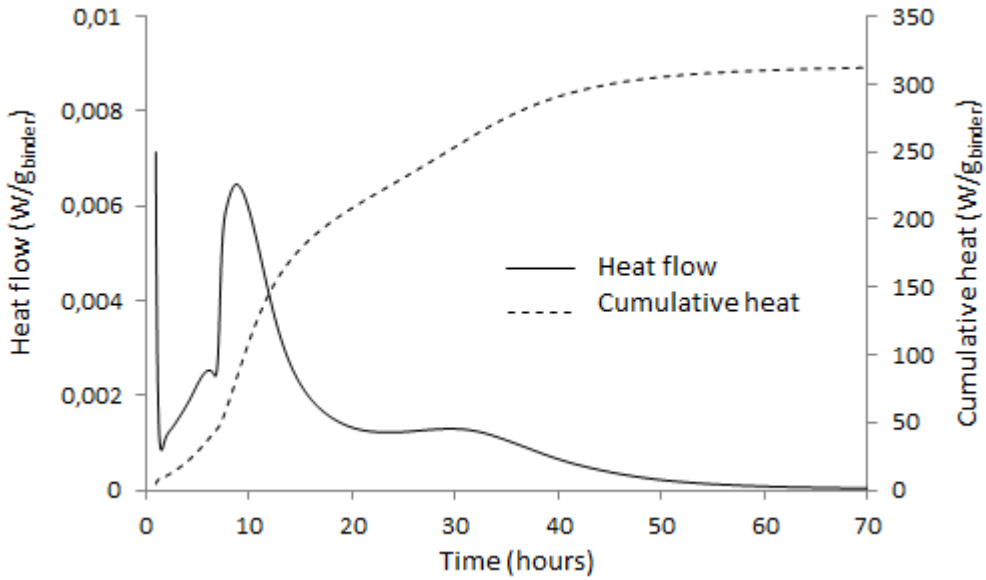

Figure 10 : Heat flow and cumulated heat of ES2 hydration

Hydration evolution

The physicochemical evolution of ES2 paste was followed by sampling and characterization tests during hydration. The samples after 1, 9 and 28 days of hydration were characterized by XRD and TGA (Figure 11 and Figure 12). Characteristic peaks of ettringite (e.g. 9.721 Å - 2θ = 10.6°) appeared after 1 day, as did the decrease in the intensity of peaks of anhydrous phases (ye'elimite and anhydrite). In fact, an intensification of ettringite peaks over time and a decrease in the intensity of anhydrous peaks were noted up to 28 days. However, the presence of ye'elimite and anhydrite peaks visible on the XRD diagram after 28 days of hydration means that hydration was not completed. The minor phases, periclase and fluorellestadite, of ES2 were assumed to be inert phases.

Secondary phases such as belite (d = 2.783 Å - 2θ Co Kα = 37.5°) were still present, meaning that there was little or no reaction at that age. It is recognized that the kinetics of dissolution of C_2S is low in relation to those of ye'elimite or anhydrite [62,68]. The phases of stratlingite ($2CaO.Al_2O_3.SiO_2.8H_2O$) and AFm ($3CaO{\cdot}Al_2O_3{\cdot}CaSO_4{\cdot}12H_2O$), predicted by thermodynamic simulation, were not detected by XRD. An additional test with an electron probe microanalyser detected traces of AFm in the ES2 matrix. Details are given in the "Traces of stratlingite and AFm" section.

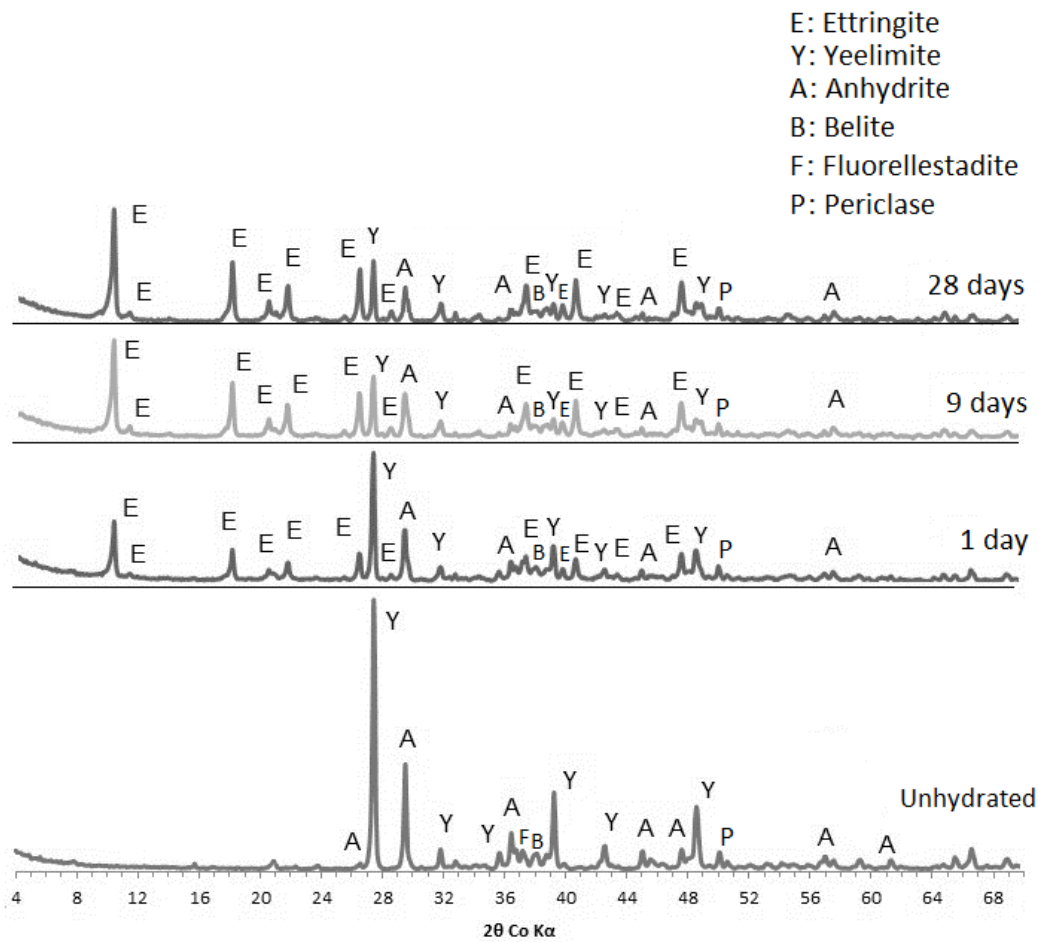

Figure 11 : X-ray diffraction of ES2 hydrated for 1, 9 and 28 days

The simulation of hydration (Figure 7) predicted the formation of aluminium hydroxide ($Al(OH)_3$), which did not appear in the XRD diagram (Figure 9), but this phase can precipitate in crystallized and/or amorphous forms. The thermogravimetric analysis (Figure 12) confirmed the presence of this phase (in amorphous form, it was not visible on the XRD diagram), and also quantified it over time of hydration. Thus, the crystallized phase of $Al(OH)_3$ (gibbsite) was not observed in the ES2 matrix. The exothermic peaks characterizing dehydration of ettringite and aluminium hydroxide $Al(OH)_3$ appeared around 130 °C and 270 °C, respectively (Figure 12). However, there was a shift in decomposition temperature with the sample age. This shift, observed in the literature [62,69], could be related to the fact that the amount of hydrate increased with the hydration time. Consequently, the quantity of dehydrated water (TGA water loss) increased, leading to a broadening of the DTG peak.

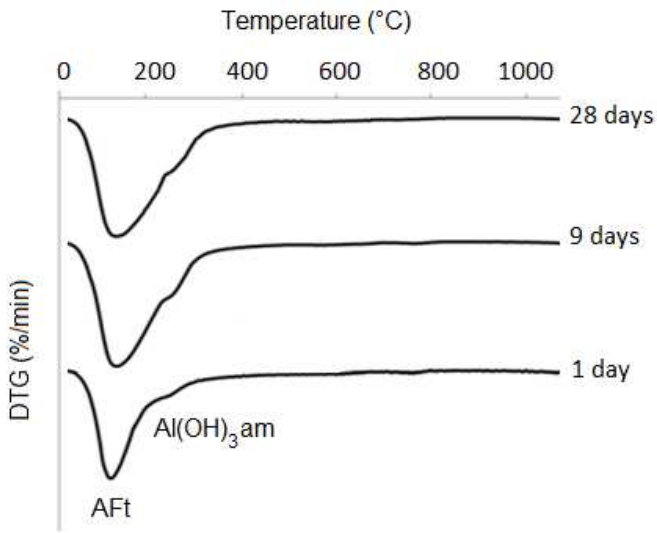

Figure 12 : Thermogravimetric analysis of ES2 after 1, 9 and 28 days of hydration

Amount of hydrate and reaction rate - AFt and $Al(OH)_3$

The quantity of hydrates was calculated from the TGA mass loss, after deconvolution of the DTG peaks. The results of the quantification of ettringite and amorphous $Al(OH)_3$ are shown in Figure 13. Rapid hydration kinetics of the cement was noted in the short term, since 35% ettringite was produced during the first day of hydration (Figure 13). After 1d, ettringite content continued to increase, but the hydration kinetics slowed down between the 9th and the 28th days. An ettringite content of 53% was reached after 28 days of hydration, instead of 70% at complete theoretical hydration according to equation 2. XRD analysis (Figure 11) shows that hydration was not complete, since there was still ye'elimite and anhydrite present at 28 d. This could be explained by the fact that CSA clinker grains were not fine enough to react completely. This was probably confirmed by the SEM observation of the sample after 28 days of hydration, since CSA clinker grains were observed (Figure 14). The primary ettringite precipitated around the clinker grains and probably blocked further hydration. In order to verify this assumption, the 28-day-old sample was milled to 7200 cm^2/g (Blaine) and rehydrated under water for 4 days. An ettringite content of 66% (i.e. a hydration rate of 94%) was reached after 4 days of rehydration (Figure 13). This result means that the particles of the cement were too large to allow complete hydration of the CSA. Note that the thermodynamic modelling did not consider factors that could change the kinetics of dissolution of the anhydrous phase, like the fineness of the binder for example. However, the presence of anhydrite after 28 days in the CSA paste was difficult to explain. According to Le Saout et al. [70], this behaviour could be partly explained by the presence of $Al(OH)_3$ around the anhydrous gains. It is necessary to supplement this approach with additional SEM analysis on a polished section.

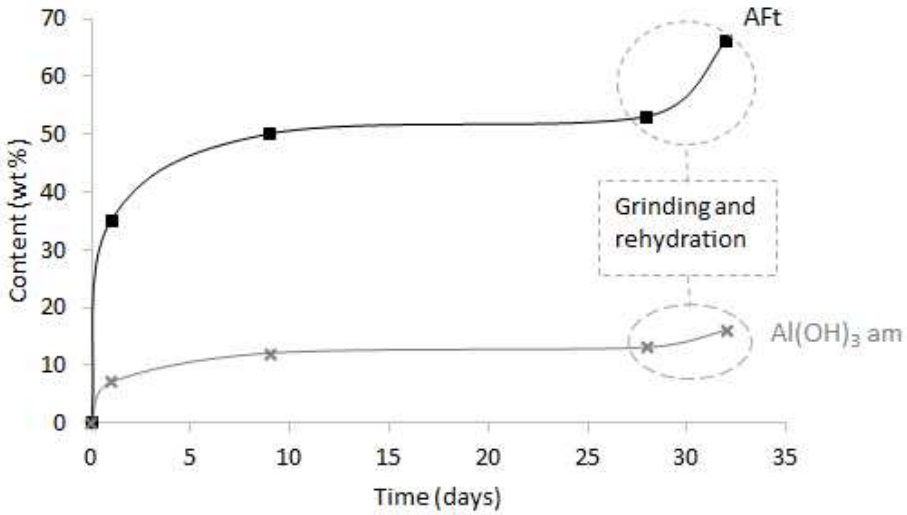

Figure 13 : Ettringite (AFt) and $Al(OH)_3$ contents in ES2

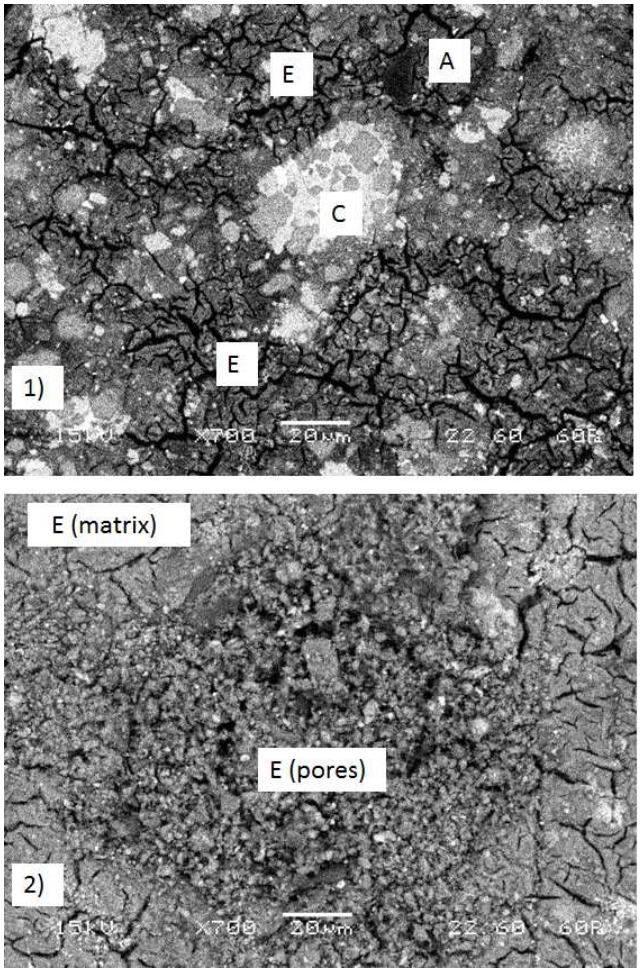

Figure 14 : SEM image of non-ground ES2 hydrated for 28 days (1) then ground and rehydrated for 4 days after 28 days (2) (A: amorphous $Al(OH)_3$, E: ettringite, C: sulfoaluminate clinker)

Traces of stratlingite and AFm

Thermodynamic simulations predicted the precipitation of two other hydrates besides AFt: stratlingite ($2CaO.Al_2O_3.SiO_2.8H_2O$) and AFm ($3CaO{\cdot}Al_2O_3{\cdot}CaSO_4{\cdot}12H_2O$). In contrast, these two phases were not detected by XRD and TGA. Electron probe microanalysis detected traces of AFm in the ES2 matrix (Figure 15), which was due to calcium sulfate (anhydrite) deficiency in the pore solution. The AFm was produced according to Equation 9. The simulation showed AFm precipitation after a high consumption of calcium sulfate to form AFt (Figure 9). Furthermore, probable local sulfate deficiencies were observed in the matrix. The mixture cannot have been completely homogeneous since the anhydrite was added after firing and grinding of the sulfoaluminate clinker. The presence of $Al(OH)_3$ around the anhydrite grains [70] could also have led to sulfate deficiencies.

The absence of AFm characteristic on the XRD diagrams may have been due to the small amount produced but also to the possibility that its structure was poorly crystallized. According to Zhou and Glasser [39], an excess of sulfate in the AFm composition generates an amorphous structure (not visible in an XRD diagram). Furthermore, it is showed the generation AFm is promoted with curing temperature rising [37].

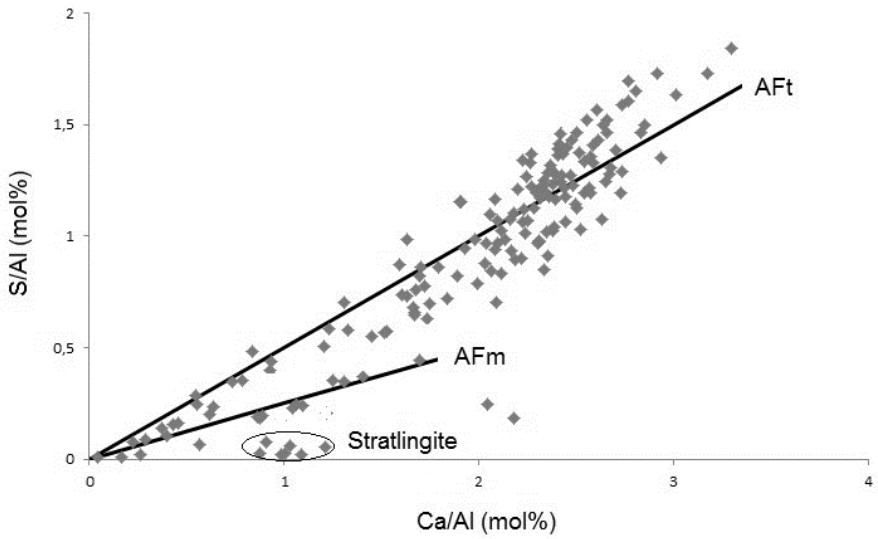

Figure 15 : Electron probe microanalysis of ES2 hydrated for 28 days

In addition, a number of points taken to be stratlingite ($2CaO.Al_2O_3.SiO_2.8H_2O$) were also observed in Figure 15. This was confirmed by SEM observation of the same samples (Figure 16). The formation of this crystal required a silicon source and was probably the result of hydration of the belite ($2CaO,SiO_2$), a secondary phase of ES2, according to Equation 10. A low mass content (8%) of belite (C_2S) was present in the anhydrous ES2 and had low dissolution kinetics compared to ye'elimite. Therefore, the precipitation kinetics of stratlingite was very slow compared to that of ettringite.

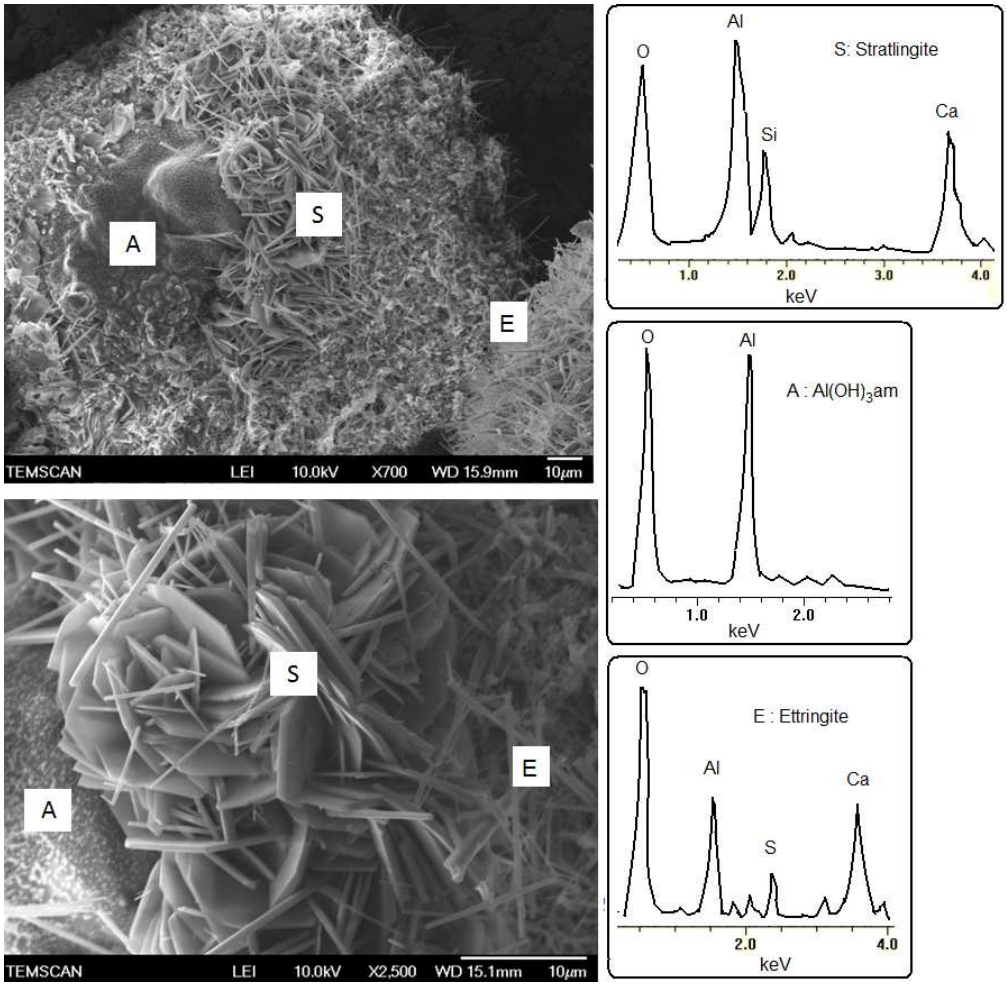

Figure 16 : SEM images of stratlingite in ES2 paste after 28 days of hydration
(A: amorphous $Al(OH)_3$, S: stratlingite)

Analysis of samples after one year of hydration showed that belite continued to react beyond 28 days, since a production of stratlingite was detectable by DRX ($2\theta = 8°$, Figure 17). This product was not yet visible on the diffractogram of the 28 days ES2 paste (Figure 11). It should be noted that it was also possible to distinguish a characteristic AFm peak with low intensity (Figure 17).

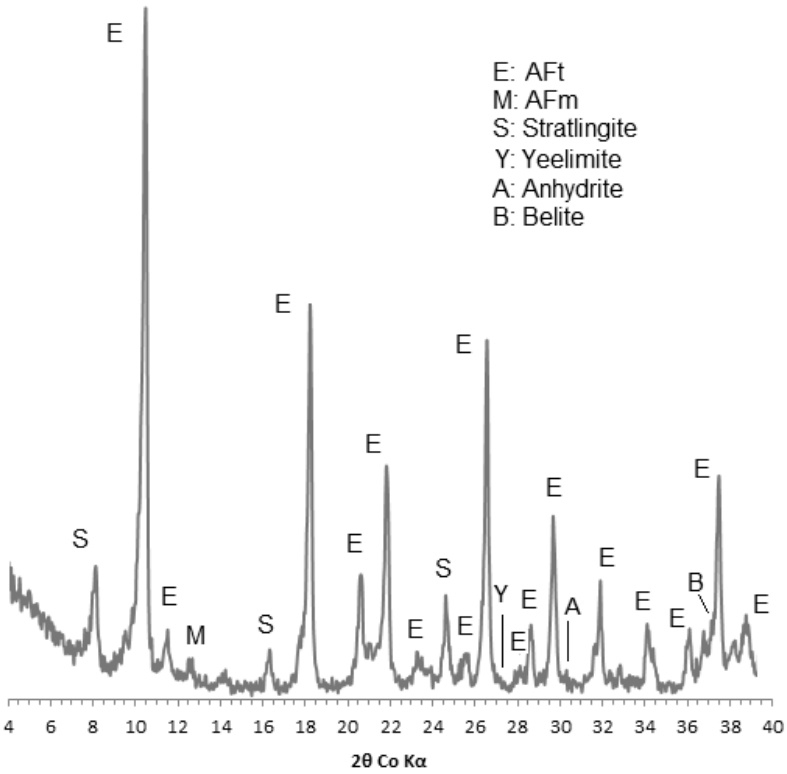

Figure 17 : XRD diagram after one year of ES2 hydration

Hydration of ground ES2

The ES2 was ground to a Blaine specific surface area of 7200 cm^2/g before the hydration started, in order to improve the rate of reactions. As expected, the hydration kinetics was increased. An AFt mass content of 68% was reached at 28 days (hydration rate of 97% relative to the expected theoretical value), which was close to the theoretical value calculated in stoichiometric condition (70% according to Equation 2). While the thermodynamic model (Figure 9) predicted an ettringite content of 61%, this model/experimental difference of 7% was probably due to the error in TGA measurement on the one the hand and, on the other hand, the fact that the dissolution kinetics were determined from the area of XRD peaks of anhydrous phases (semi-quantification). The Rietveld quantification method would be more rigorous in determining the dissolution kinetics of the anhydrous phase. Thus, the grinding of calcium sulfoaluminate binder before starting the hydration allowed almost complete hydration after 28 days, that is to say the calculated ettringite content if all ye'elimite contained in the ES2 reacted in stoichiometric conditions according to Equation 2. Moreover, the SEM images of the ground ES2 samples show the absence of anhydrous grains (Figure 18).

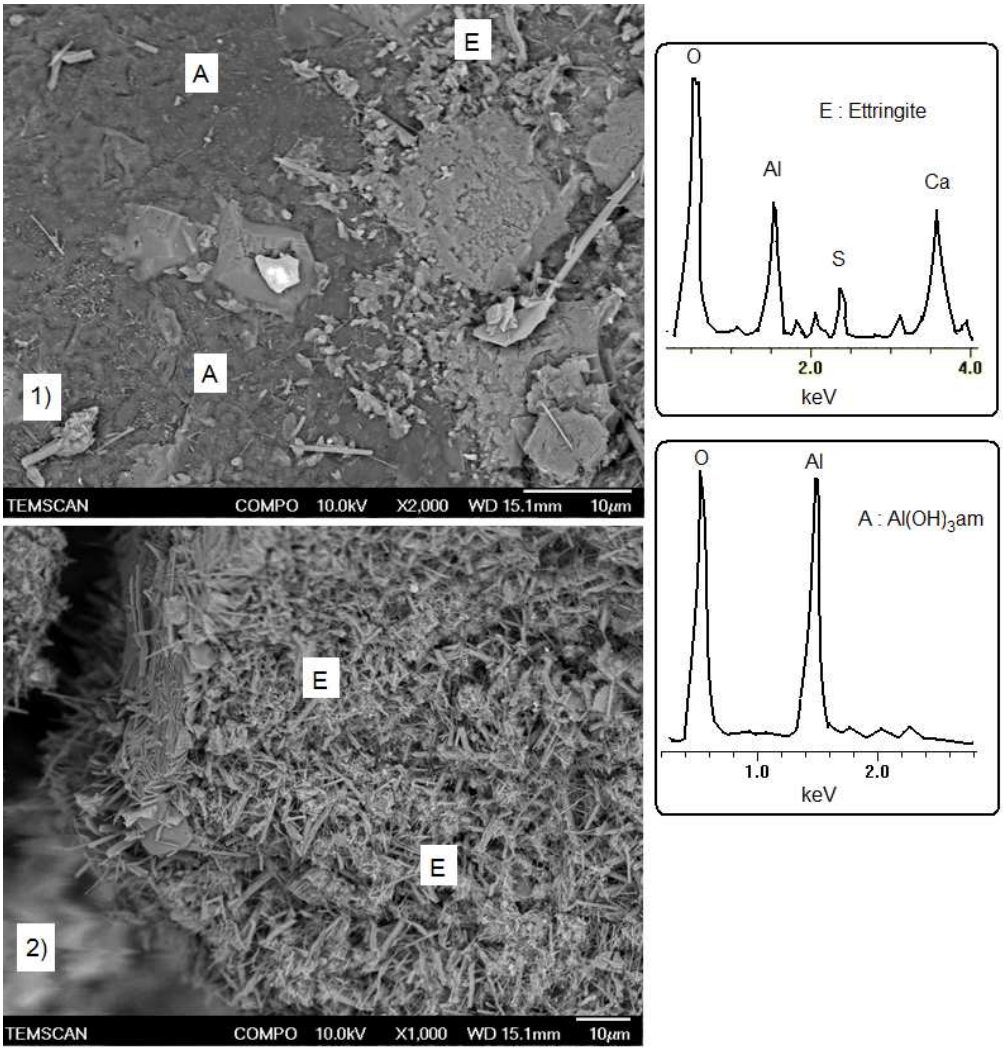

Figure 18: SEM image of non-ground ES2 (1) and ES2 ground to 7200 cm^2/g (2), both hydrated for 28 days*?* (A: amorphous $Al(OH)_3$, E: ettringite)

ES2 Stability

Structural stability is a very important criterion for the choice of a storage material. As shown in Figure 19, the ES2 paste structure was stable at the macroscopic scale after 28 days of hydration. This structural stability was maintained after 28 days, as no macro-cracks were detected even after one year of hydration. This could be explained by the fact that the amount of anhydrite in ES2 was below the critical threshold of calcium sulfate content that causes volume instability and macroscopic cracking of the CSA paste. This critical threshold of calcium sulfate in the CSA was 56 mol% according to Bizzozero et al. [31]. These authors found an increase in the crystallization pressure with the calcium sulfate content, leading to expansion.

Figure 19 : Sample of ES2 after 28 days of hydration

Mechanical properties of ES2

Unlike ES1, ES2 paste has a volume stability that allows it to develop increasing compressive strength over the time of hydration (Figure 20). The compressive strength increased with the ettringite content and 32 MPa was reached after 28 days of hydration. This mechanical resistance also increased in the long term, with 41 MPa after one year, while the ettringite content remained constant. This strength increase in the long term may be related to stratlingite precipitation, even though the ettringite content remains the key parameter justifying the strength development of CSA based materials [67].

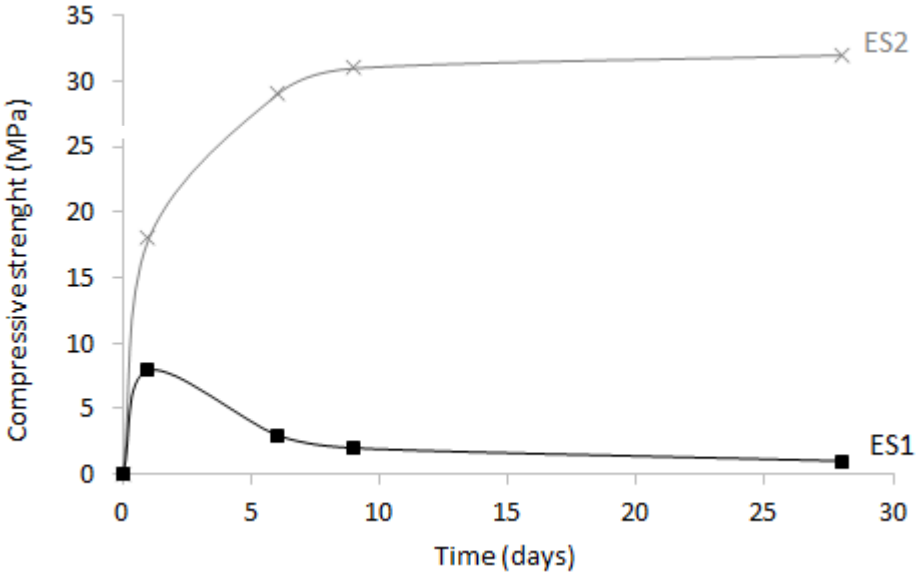

Figure 20 : Compressive strength of ES2 paste

3.2.3 Ettringitic systemES2 outcome

In accordance with the thermodynamic simulation, the hydration of ES2 formed AFt (68%) that was stable in the short and long term, with a coproduction of amorphous $Al(OH)_3$ from the reaction of ye'elimite and anhydrite. Traces of secondary hydrates (AFm and stratlingite) were detected in the long term.

Thermodynamic modelling was generally in agreement with experiment. It allowed the CSA binder composition to be optimized before beginning hydration, the hydration mechanism to be better understood, stable phases (ettringite ...) to be identified, their temporal evolution to be explained, and semi-quantification to be carried out.

The choice of ES2 paste as a heat storage material was motivated by its high ettringite content (68%) and its dimensional stability. However, this material has a high density, which reduces the accessibility of water molecules to that of ettringite (AFt). To overcome this structural problem, the porosity and permeability of the paste must be increased in order to improve the heat storage capacity of the material.

3.3 Improved storage material: aerated ettringitic system(AES2)

The heat charging phase was carried out by endothermal desorption (and dehydration) of the ettringite based material, while the heat discharging phase was characterized by adsorption of water vapour into the porous network of the material (and rehydration). Thus, in order to use the ettringitic systemES2 as a heat storage material, it was necessary to improve its permeability so as to enhance the diffusion of water vapour in the material and facilitate exchanges between water and ettringite molecules. Furthermore, ES2 paste contained a large amount of ettringite with low permeability and low porosity. This is characteristic of CSA based materials [37]. To overcome this structural problem, the CSA paste permeability had to be increased. To do this, the ettringitic systemES2 was aerated by the addition of aluminium powder and calcium hydroxide ($Ca(OH)_2$). The reaction of the latter released hydrogen gas, which increased the volume of the paste and generated porosity (Equation 3). The foaming process has been described in section 3.

3.3.1 Structural properties

The resulting aerated ettringitic system(AES2) contained 68 wt% of AFt (TGA). It had high porosity at the macroscopic (Figure 21) and microscopic (Figure 22) scale. The aerated ettringitic system(AES2) was observed to have a much less dense matrix than the non-aerated material (ES2 paste) (Figure 21).

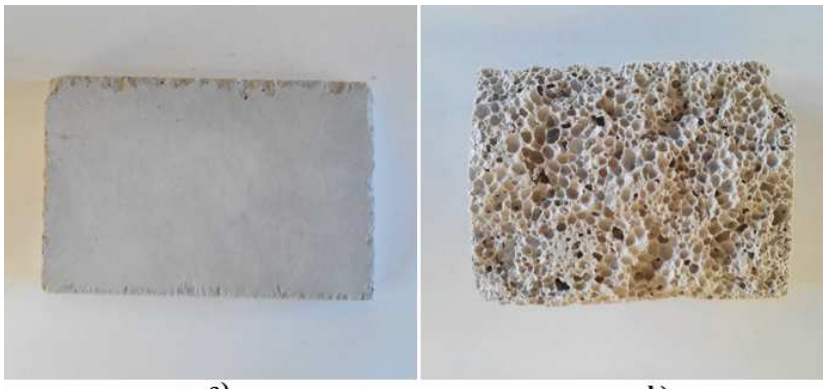

a) b)

Figure 21 : Samples of ES2 (a) and AES2 (b) hydrated for 28 days

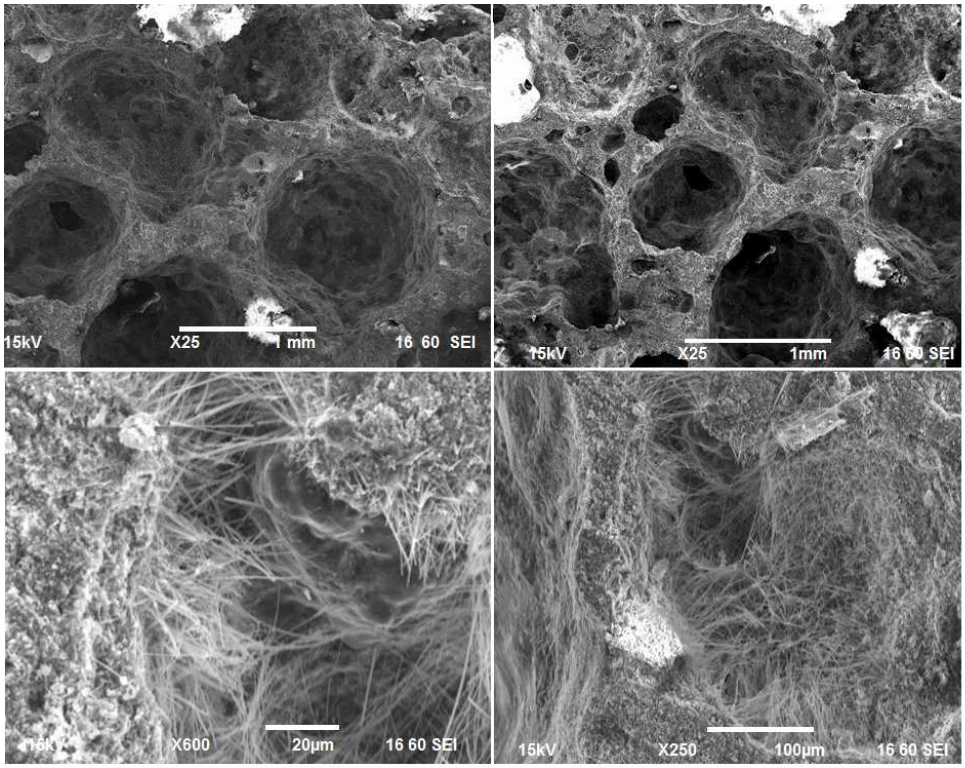

Figure 22 : SEM image of AES2 porous network

Table 3 shows the improvement in the transfer properties of the aerated material (AES2) relative to the ES2 material. The foaming process increased the porosity accessible to water by 62% (from 14% to 76%) and the gas permeability by a factor of 250. This was beneficial to the water vapour diffusion into the material (mass transfer) during the charging phase (desorption and dehydration) and discharging phase (adsorption and rehydration). The stored energy was directly related to the amount of water adsorbed. Thus, the increase in the adsorption sites of the material improved its energy performance. Furthermore, volume expansion was not observed on the aerated material (AES2) probably because of the low crystallization pressure due to the high macroporosity and the low calcium sulfate content related to the critical threshold. The critical threshold of calcium sulfate in the CSA was 56 mol% to avoid ettringite swelling par crystallization pressure, according to Bizzozero et al. [31].

Table 3 : Intrinsic gas permeability, porosity accessible to water and compressive strength of non-aerated material (ES2) and aerated material (AES2)

Material	Permeability (m^2)	Porosity (%)	Compressive strength (MPa)
Non-aerated material (ES2)	$3.6 \cdot 10^{-16}$	14%	32
Aerated material (AES2)	$8.8 \cdot 10^{-14}$	76%	2

However, the compressive strength of ES2 decreased significantly with the increase of porosity (Table 4). After 28 days of hydration, the compressive strength of ES2 and that of the improved material AES2 were 32 MPa and 2 MPa, respectively. The mechanical strength of

cellular concrete increases with its density [10,35-36]. However, this low compressive strength of AES2 (2 MPa) was sufficient for a self-supporting structure. This is an important advantage in relation to the existing storage material. In fact, the existing storage materials are used in the form of a powder bed for thermal energy storage systems of buildings [12–16], but the powder bed without mechanical strength have not a self-supporting capacity. Furthermore, mechanical strength could be improved by adding sand and/or gravel, thus reducing the W/C ratio. The storage material optimization in terms of mechanical strength will be performed in accordance to application (for example supporting structure with heat storage capacity).

3.3.2 Reversibility properties

To study the reversibility of the storage process at 60°C, cycles of dehydration (heat charge) and rehydration (heat discharge) were performed in the laboratory. Three cylindrical samples of aerated CSA paste (D = 11 cm, L = 5 cm) were used. During the dehydration phase (heat storage), samples were stored at 60°C for 3 days in a vacuum desiccator. Sensors into the desiccator showed a low relative humidity (between 3% and 8%). In this condition, ettringite (30 H_2O molecules) was converted to metaettringite (12 H_2O molecules). The rehydration phase was carried out by immersing the samples in water at 20°C. The mass evolution was followed by weighing the specimens over time. However, each weighing operation during the hydration stage was preceded by a drying of the saturated samples at 40°C for 2h to remove not only free water in the pores but also zeolitic water (decrease of water content per ettringite molecule from 32 H_2O to 30 H_2O molecules). This preheating of samples before weighing allowed us to measure exclusively water from rehydration. Isothermal dehydration at 60°C for 3 days led to a sudden fall in the material mass until 25% had been lost, which was an invariant level even if the heating period was extended (Figure 23). At this stage, analysis of dehydrated samples indicated the absence of ettringite and the presence of metaettringite. This isothermal heating at 60°C caused the conversion of ettringite to metaettringite. The subsequent rehydration phase was characterized by the gradual recovery of the mass of the samples (Figure 23). The analysis of humidified samples confirmed the conversion of metaettringite to ettringite by hydration. Thus, the conversion of ettringite to metaettringite is reversible during 1 cycle of heat storage. No macroscopic cracks of collapse were observed on the dehydrated and rehydrated samples, the compressive strength is not decreased. The reversibility of a heat storage cycle (dehydration-rehydration) is proven, but the conservation of material energy density requires reversibility after several dehydration-hydration cycles. So, after this first cycle, six successive cycles (dehydration rehydration) were performed with the same samples (Figure 23). After 7 charging/discharging cycles, no macroscopic cracks of collapse were observed on the samples, this was confirmed by the conservation of the compressive strength around 2MPa.

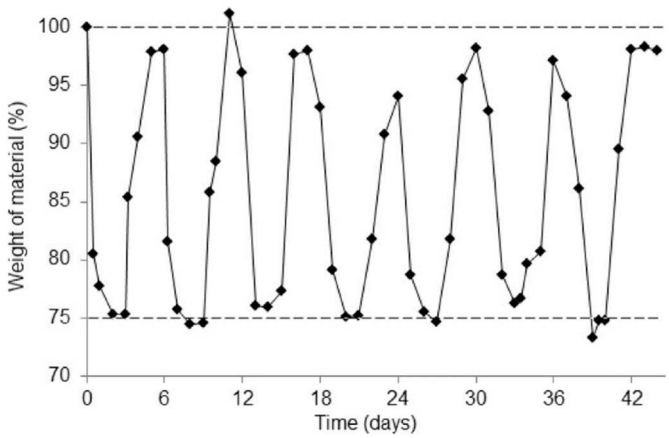

Figure 23 : Mass variation of AES2 during 7 cycles of dehydration and rehydration

3.3.3 Heat storage properties

To evaluate the heat storage capacity of the aerated material, a prototype where a single gas (nitrogen) in direct contact with the ettringite material porosity served as the heat transfer fluid in the charging phase and as the humidifying gas in the discharging phase (Figure 24). To perform the storage tests in the laboratory, the reactor was connected to a heater and a humidifier to simulate heat charging and discharging, respectively. The heater was only used during the charging phase and the humidifier only hydrated the material during the discharging phase. The {reactor + heat source + source of moisture} set formed the heat storage system. The test bed installed in the laboratory reproduced the functioning of the system. The reactor was a cylindrical thermochemical adsorber, 16 cm in diameter and 32 cm long. It consisted of aerated ettringite system (AES2) insulated from steam or water by a PVC cylinder (Figure 24). To avoid heat loss, the reactor was thermally insulated from its surroundings by a 10 cm thick layer of glass wool and a thin layer of polystyrene at the surface.

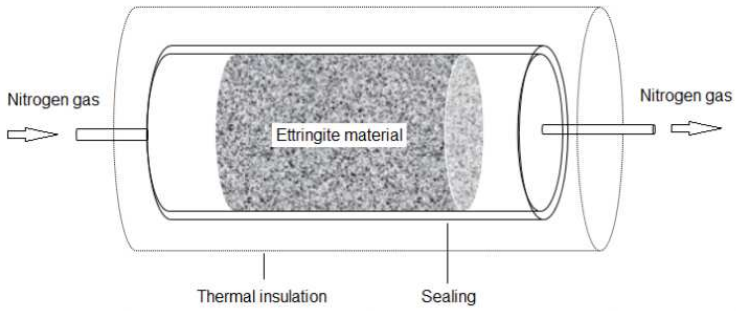

Figure 24 : Operating diagram of the second prototype thermochemical reactor

During the heat charging phase, the electric heating system was used to heat the dry nitrogen as in a solar collector and the resulting hot gas (60°C) passed through the porosity of the material [9]. The dehydration of the material led to the heat storage. This period lasted for about 3 days for this prototype size (4.4 l, 1.8 kg). The heat stored was not restored as long as the ettringite material was isolated from water (vapor or liquid). Unlike in sensitive or latent storage systems, thermal insulation of the ettringite material was not required during the

intermediate phase between charging and discharging. Heat storage could be short-term (for days or weeks) or long-term (seasonal) [7]. The chemical part of the storage process (endothermic dehydration) was related to the conversion of ettringite to metaettringite by the loss of 18 molecules of water per molecule of ettringite (Figure 25).

Charging	Ettringite (30 H_2O) + Heat → Metaettringite (12 H_2O) + Water (18 H_2O)
Discharging	Metaettringite (12 H_2O) + Water (18 H_2O) → Ettringite (30 H_2O) + Heat

Figure 25 : Reactions of ettringite - metaettringite conversion

In the discharging phase, a humidification system consisting of a water bubbler was used to charge the gas (nitrogen) circulating through it with water vapor. This humidified gas passed through the permeable porous material, which adsorbed water vapor (physical reaction) and then hydrated (chemical reaction). This generated an exothermic reaction (Figure 25) and the restored heat was transported by the heat transfer fluid (nitrogen). During this phase of heat recovery, the cold, humidified gas (inlet nitrogen) became hot and dry (outlet nitrogen). The heat storage yield, the ratio of discharged heat to charged heat, was 71%, with a storage density of 117 kWh/m^3 (Figure 26). The prototype was not only simpler in terms of operation, but also more efficient in terms of heat storage performance than other thermochemical prototypes using hydrate salts [13].

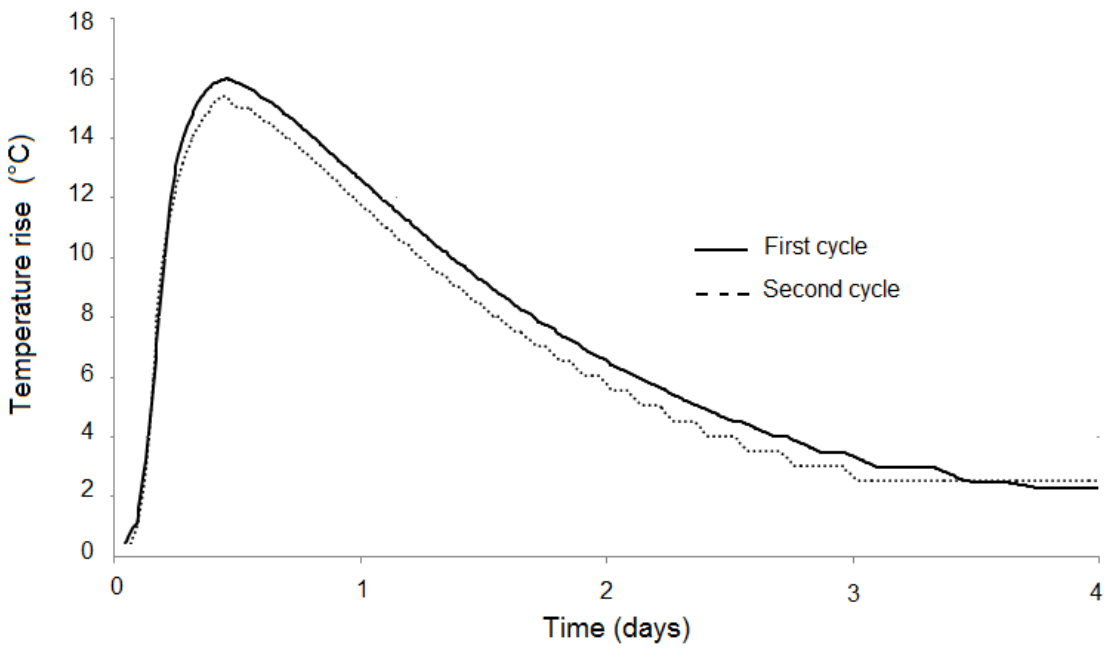

Figure 26: Heat restitution during discharging phase of two successive cycles.

The temperature and relative humidity sensors placed in cylindrical reactor prototype were used to measure the hydrothermal evolution into the ettringite material during complete storage cycle. The results (Figure 26) confirmed the thermal reversibility of the released heat over 2 complete cycles.

4 Conclusion

The aim of this paper was to describe the development of an ettringite based material capable of storing thermal energy by the thermochemical reaction of ettringite and water. The ettringitic systembased on CSA was hydrated with (ES1) and without (ES2) hydrated lime to produce ettringite. The ES1 and ES2 pastes contained 43% and 68% of ettringite respectively after 28 days of hydration. The study of these CSA-based materials showed that:

- The ettringitic systemhydrated with hydrated lime (ES1) under water reached only 43% of ettringite (instead of the theoretical 95%), with a cracked structure. However, the ettringitic systemwithout hydrated lime under water (ES2) reached 68% ettringite at 28 days (instead of the theoretical 70%), with a very stable solid structure and low porosity and permeability.

- Thermodynamic modelling of the ES2 hydration (ettringitic systemwithout hydrated lime) allowed us to predict the temporal evolution of ES2 composition, to fully understand the hydration mechanism causing dissolution of anhydrous phases and precipitation of hydrates, and also to identify stable phases (ettringite, etc.). Thermodynamic modelling was in agreement with experiment.

- The fineness (Blaine) of the CSA binder increased its hydration kinetics, allowing a high hydration rate after 28 days.

- The permeability of the ES2 paste was increased by adding aluminium powder (chemical foaming) into the raw material before hydration in order to improve its heat storage capacity by promoting exchanges between ettringite and water molecules.

Ettringite material synthesized and then aerated by foaming (AES2) can be used as a monolithic thermochemical storage material for buildings. This aerated material satisfied the main criteria for a storage material: high ettringite content to increase the heat storage density, high permeability to promote the exchange between water and ettringite molecules, and mechanical strength to provide self-supporting capacity. AES2 was used as storage material in cement paste form with a heat storage capacity of 117 kWh/m^3 but ettringite systems can be used in the form of mortar or concrete in buildings. Depending on the mechanical requirements of the construction, the storage material can be used as a self-supporting structure or even a load bearing structure if its mechanical strength is sufficient.

5 References

[1] Energy Efficiency Plan 2011, Energy Efficiency Plan 2011, COM 109(4).

[2] L.J. Struble, P.W. Brown, Heats of dehydration and specific heats of compounds found in concrete and their potential for thermal energy storage, Sol. Energy Mater. 14 (1986) 1-12.

[3] F. Winnefeld, J.P. Kaufmann, Concrete produced with calcium sulfoaluminate cement – a potential system for energy and heat storage, First Middle East Conference on Smart Monitoring. Assessment and Rehabilitation of Civil Structures, Dubai, UAE, 2011.

[4] Van Berkel J, Solar thermal storage techniques. Research commissioned by The Netherlands Agency for Energy and the Environment NOVEM (2000) project # 143.620-935.8.
[5] M. Cyr, S. Ginestet, K. Ndiaye, Energy storage/withdrawal system for a facility, Pat. WO 2017089698 A1, 2015.
[6] K. Ndiaye, Etude numérique et expérimentale du stockage d'énergie par les matériaux cimentaires (Doctorate/Ph.D.), LMDC - Université de Toulouse, 2016.
[7] K. Ndiaye, S. Ginestet, M. Cyr, Modelling and experimental study of low temperature energy storage reactor using cementitious material, Appl. Therm. Eng. 110 (2017) 601–615.
[8] Ndiaye K., S. Ginestet, M. Cyr, Durability and stability of an ettringite-based material for thermal energy storage at low temperature, Cem. Concr. Res. 99 (2017) 106-115.
[9] K. Ndiaye, S. Ginestet, M. Cyr, Experimental evaluation of two low temperature energystorage prototypes based on innovative cementitious material, Appl. Energy 217 (2018) 47–55.
[10] K. Ndiaye, S. Ginestet, M. Cyr, Thermal energy storage based on cementitious materials: a review, AIMS Energy 6 (2018) 97–120.
[11] B. Chena, F. Kuznika, M. Horgnies, K. Johannes, V. Morin, E. Gengembre, Physicochemical properties of ettringite/meta-ettringite for thermal energy storage: Review, Sol. Energy Mater. Sol. Cells 193 (2019) 320-334.
[12] D.M. Ruthven, Principles of adsorption and adsorption processes. Wiley Interscience, New York,1984.
[13] B. Michel, N. Mazet, P. Neveu, Experimental investigation of an innovative thermochemical process operating with a hydrate salt and moist air for thermal storage of solar energy: Global performance, Appl. Energy 129 (2014) 177–186.
[14] S. Hongois, F. Kuznik, P. Stevens, J.J. Roux, Development and characterization of a new $MgSO_4$–zeolite composite for long-term thermal energy storage, Sol. Energy Mater. Sol. Cells 95 (7) (2011) 1831-1837.
[15] A. Fopah-Lele, J.G. Tamba, A review on the use of $SrBr_2 \cdot 6H_2O$ as a potential material for low temperature energy storage systems and building applications, Sol. Energy Mater. Sol. Cells 164 (2017) 175–187.
[16] Z. Ma, H. Bao, A.P. Roskilly, Study on solidification process of sodium acetate trihydrate for seasonal solar thermal energy storage, Sol. Energy Mater. Sol. Cells 172 (2017) 99-107.
[17] L.M. Sun, Y. Feng, M. Pons, Numerical investigation of adsorptive heat pump systems with thermal wave heat regeneration under uniform-pressure conditions, Int. J. Heat Mass Transfer 2 (1997) 281–293.
[18] A. Mhimid, Theoretical study of heat and mass transfer in a zeolite bed during water desorption: validity of local thermal equilibrium assumption, Int. J. Heat Mass Transfer 41 (1998) 2967–2977.
[19] K.C. Leong, Y. Liu, Numerical modeling of combined heat and mass transfer in the adsorbent bed of a zeolite/water cooling system, Appl. Therm. Eng. 24 (2004) 2359–2374.
[20] Duquesne M, Toutain J, Sempey A, S. Ginestet, E. Palomo del Barrio, Modeling of a nonlinear thermochemical energy storage by adsorption on zeolites, Appl. Therm. Eng. 71 (2014) 469–480.
[21] D. Alby, F. Salles, J. Fullenwarth, J. Zajac, On the use of metal cation-exchanged zeolites in sorption thermochemical storage: Some practical aspects in reference to the mechanism of water vapor adsorption, Sol. Energy Mater. Sol. Cells 179 (2018) 223-230.

[22] B. Xu, Z. Li, Performance of novel thermal energy storage engineered cementitious composites incorporating a paraffin/diatomite composite phase change material, Appl. Energy 121 (2014) 114–122.
[23] S.A. Memon, H.Z. Cui, H. Zhang, F. Xing, Utilization of macro encapsulated phase change materials for the development of thermal energy storage and structural lightweight aggregate concrete, Appl. Energy 139 (2015) 43–55.
[24] Y. Zhang, K. Wang, W. Tao, D. Li, Preparation of microencapsulated phase change materials used graphene oxide to improve thermal stability and its incorporation in gypsum materials, Constr. Build. Mater. 224 (2019) 48 -56.
[25] P. Sukontasukkul, P. Uthaichotirat, T. Sangpet, K. Sisomphon, M. Newlands, A. Siripanichgorn, ,P. Chindaprasirt, Thermal properties of lightweight concrete incorporating high contentsof phase change materials. Constr. Build. Mater. 207 (2019) 431-439.
[26] X. Wang, H. Yu, L. Li, M. Zhao, Experimental assessment on the use of phase change materials (PCMs)-bricks in the exterior wall of a full-scale room. Energ. Convers. Manage. 120 (2016) 81–89.
[27] A. Marani, M.L. Nehdi, Integrating phase change materials in construction materials: Critical review. Constr. Build. Mater. 217 (2019) 36-49.
[28] R.K. Sharma, P. Ganesan, V.V. Tyagi, H.S.C. Metselaar, S.C. Sandaran, Developments in organic solid–liquid phase change materials and their applications in thermal energy storage. Energ Convers. Manage. 95 (2015) 193–228.
[29] T. Nishikawa, K. Suzuki, S. Ito, K. Sato, T. Takebe, Decomposition of synthesized ettringite by carbonatation, Cem. Concr. Res. 22 (1992) 6-14.
[30] I. Odler, Special inorganic cements, CRC Press, 2000 (416 pp.).
[31] J. Bizzozero, C. Gosselin, K.L. Scrivener, Expansion mechanisms in calcium aluminate and sulfoaluminate systems with calcium sulfate, Cem. Concr. Res. 56 (2014) 190–202.
[32] J. Péra, J. Ambroise, New application of calcium sulfoaluminate cement, Cem. Concr. Res. 34 (4) (2004) 557-562.
[33] C. Cau Dit Coumes, S. Courtois, S. Peysson, J. Ambroise, J. Péra, Calcium sulfoaluminate cement blended with OPC: a potential binder to encapsulate low-level radioactive slurries of complex chemistry, Cem. Concr. Res. 39 (9) (2009) 740-747.
[34] F. Winnefeld, S. Barlag, Calorimetric and thermogravimetric study on the influence of calcium sulfate on the hydration of ye'elimite, J. Therm. Anal. Calorim. 101 (2010) 949–957.
[35] N. Narayanan, K. Ramamurthy, Structure and properties of aerated concrete: a review, Cem. Concr. Compos. 22 (5) (2000) 321-329.
[36] G. Samson, A. Phelipot-Mardelé, C. Lanos, A review of thermomechanical properties of lightweight concrete. Mag. Concr. Res. 69 (2017) 201–216.
[37] L. Li, R. Wang, S. Zhang, Effect of curing temperature and relative humidity on the hydrates and porosity of calcium sulfoaluminate cement. Constr. Build. Mater. 213 (2019) 627-636.
[38] Q. Zhou, E.E. Lachowski, F.P. Glasser, Metaettringite, a decomposition product of ettringite, Cem. Concr. Res. 34 (4) (2004) 703-710.
[39] Q. Zhou, F.P. Glasser, Thermal stability and decomposition mechanisms of ettringite at < 120 °C, Cem. Concr. Res. 31 (9) (2001) 1333–1339.
[40] L.G. Baquerizo, T. Matschei, K.L. Scrivener, Impact of water activity on the stability of ettringite, Cem. Concr. Res. 79 (2016) 31–44.

[41] M. Cyr, P. Rivard, F. Labrecque, A. Daidié, High-pressure device for fluid extraction from porous materials: application to cement-based materials, J. Am. Ceram. Soc. 91 (8) (2008) 2653-2658.
[42] J. Havlica, S. Sahu, Mechanism of ettringite and monosulphate formation, Cem. Concr. Res. 22 (4) (1992) 671-677.
[43] M. Su,Y. Wang, L. Zhang, D. Li, Preliminary study on the durability of sulfo/ferro-aluminate cements, in: Proceedings 10th ICCC, Goteborg, Sweden, 1997.
[44] K. Ogawa, D.M. Roy, $C_4A_3\overline{S}$ hydration, ettringite formation, and its expansion mechanism: II. Microstructural observation of expansion, Cem. Concr. Res. 12 (1) (1982) 101-109.
[45] P.K. Mehta, Mechanism of expansion associated with ettringite formation, Cem. Concr. Res. 3 (1973) 1–6.
[46] J. Lavalle, Recherches sur la formation lente des cristaux à la température ordinaire (Research on the slow formation of crystals at ordinary temperature), C. r. hebd. séances Acad. sci. 36 (1853) 493–495.
[47] J. Bizzozero, C. Gosselin, Dimensional stability of calcium aluminate and sulfoaluminate systems, 31st Cement and Concrete Science Conference, London, UK, 2011.
[48] G.W. Scherer, Crystallization in pores, Cem. Concr. Res. 29 (1999) 1347–1358.
[49] R.J. Flatt, Salt damage in porous materials: how high supersaturations are generated, J. Cryst. Growth 242 (2002) 435–454.
[50] G.W. Scherer, Stress from crystallization of salt, Cem. Concr. Res. 34 (2004) 1613–1624.
[51] R.J. Flatt, G.W. Scherer, Thermodynamics of crystallization stresses in DEF, Cem. Concr. Res. 38 (2008) 325–336.
[52] M. Deng, M. Tang, Formation and expansion of ettringite crystals, Cem. Concr. Res. 24 (1) (1994) 119–126.
[53] D.A. Kulik, T. Wagner, F.F. Hingerl, S.V. Dmytrieva, GEM-Selektor geochemical modeling package: TSolMod library and data interface for multicomponent phase models, Can. Mineral. 50 (2012) 1173-1195.
[54] D.A. Kulik, T. Wagner, S.V. Dmytrieva, G. Kosakowski, F.F. Hingerl, K.V. Chudnenko, U. Berner, GEM-Selektor geochemical modeling package: revised algorithm and GEMS3K numerical kernel for coupled simulation codes, Computat. Geosci. 17 (2013) 1-24.
[55] B. Lothenbach, F. Winnefeld, Thermodynamic modelling of the hydration of Portland cement, Cem. Concr. Res. 36 (2) (2006) 209–226.
[56] T. Matschei, B. Lothenbach, F.P. Glasser, Thermodynamic properties of Portland cement hydrates in the system $CaO–Al_2O_3–SiO_2–CaSO_4–CaCO_3–H_2O$, Cem. Concr. Res. 37 (10) (2007) 1379–1410.
[57] B. Lothenbach, T. Matschei, G. Möschner, F. Glasser, Thermodynamic modelling of the effect of temperature on the hydration and porosity of Portland cement, Cem. Concr. Res 38 (2008) 1-18.
[58] T. Schmidt, B. Lothenbach, M. Romer, K.L. Scrivener, D. Rentsch, R. Figi, A thermodynamic and experimental study of the conditions of thaumasite formation, Cem. Concr. Res. 38 (2008) 337–349.
[59] G. Möschner, B. Lothenbach, J. Rose, A. Ulrich, R. Figi, R. Kretzschmar, Solubility of Fe-ettringite ($Ca_6[Fe(OH)_6]_2(SO_4)_3·26H_2O$), Geochim. Cosmochim. Ac. 72 (2008) 1-18.

[60] G. Möschner, B. Lothenbach, F. Winnefeld, A. Ulrich, R. Figi, R. Kretzschmar, Solid solution between Al-ettringite and Fe-ettringite ($Ca_6[Al_{1-x}Fe_x(OH)_6]_2(SO4)_3 \cdot 26H_2O$), Cem. Concr. Res. 39 (2009) 482-489.
[61] G. Le Saoût, B. Lothenbach, A. Hori, T. Higuchi, F. Winnefeld, Hydration of Portland cement with additions of calcium sulfoaluminates, Cem. Concr. Res. 43 (2013) 81–94.
[62] F. Winnefeld, B. Lothenbach, Hydration of calcium sulfoaluminate cements — experimental findings and thermodynamic modelling, Cem. Concr. Res. 40 (8) (2010) 1239-1247.
[63] P. Debye, E. Hückel, The theory of electrolytes. I. Lowering of freezing point and related phenomena, Phys. Z. 24 (1923) 185–206.
[64] C.W. Davies, Ion Association, Butterworths, Lodon, 1962: pp 37-53.
[65] B. Lothenbach, E. Wieland, A thermodynamic approach to the hydration of sulphate-resisting Portland cement, Waste Manage. 26 (7) (2006) 706–719.
[66] I.I. El-Sharkawy, B.B. Saha, S. Koyama, K.C. Ng, A study on the kinetics of ethanol-activated carbon fiber: Theory and experiments, Int. J. Heat Mass Transfer 49 (17–18) (2006) 3104-3110.
[67] M. García-Maté, A.G. De la Torre, L. León-Reina, E.R. Losilla, M.A.G. Aranda, I. Santacruz, Effect of calcium sulfate source on the hydration of calcium sulfoaluminate eco-cement, Cement Concrete Comp. 55 (2015) 53-61.
[68] J. Zhang, G. Li, W. Ye, Y. Chang, Q. Liu, Z. Song, Effects of ordinary Portland cement on the early properties andhydration of calcium sulfoaluminate cement, Constr. Build. Mater. 186 (2018) 1144-1153.
[69] J-Y Wang, Z-Z Chen, K. Wu, Properties of calcium sulfoaluminate cement made ultra-high performance concrete: Tensile performance, acoustic emission monitoring of damage evolution and microstructure, Constr. Build. Mater. 208 (2019) 767-779.
[70] G. Le Saoût, B. Lothenbach, P. Taquet, F. Winnefeld, Hydration study of a calcium aluminate cement blended with anhydrite, in: Proceedings of the fourth Conference of Calcium Aluminates International Conference, Avignon, France, 2014.